Chemical Engineering Science 295 (2024) 120192

Contents lists available at ScienceDirect

Chemical Engineering Science

journal homepage: www.elsevier.com/locate/ces

Kinetic study of propane ODH on electrospun vanadium oxide-based submicron diameter fiber catalyst

Juan José Ternero-Hidalgo, Ramiro Ruiz-Rosas, Juana María Rosas, María Olga Guerrero-Pérez, José Rodríguez-Mirasol, Tomás Cordero *

Chemical Engineering Department, Andalucía Tech, Universidad de Málaga, 29010 Málaga, Spain

ARTICLE INFO

Keywords:
Propane ODH
Mixed-oxide catalysts
Fiber catalysts
Reaction Mechanism
Kinetic study

ABSTRACT

A rigorous kinetic study of the oxidative dehydrogenation (ODH) reaction of propane on a vanadium oxide-based submicron diameter fiber catalyst has been developed. The proposed kinetic model simulates the conversion-selectivity profiles, the surface coverage of the different adsorbed species and the oxidation state of the catalyst for the studied operating conditions of temperature, space–time and inlet partial pressures of propane and oxygen. The activation energy of the rate determining step (RDS), the first hydrogen abstraction from propane, is 104 kJ·mol^{-1}. The model predicts that although the reaction seems to be pseudo-zero order with respect to oxygen in a broad range of conditions, the catalyst may not be fully oxidized during reaction. The accuracy of the model when predicting the oxidation state of the catalyst has been experimentally confirmed by analyzing the catalytic fixed bed after reaction. The reduction degree of the catalyst will depend on its intrinsic chemical nature and reaction conditions, increasing with the space–time and in detriment of the overall reaction rate. Consequently, the propane turnover frequency (TOF) will also depend on the reaction conditions and space–time, even changing along the fixed-bed reactor.

1. Introduction

The global demand for propylene is growing up since the last decades due to their use as monomers/comonomers in the petrochemical industry for the production of many interesting products (e.g. polypropylene, acrylonitrile, etc.) (Lazonby, 2023). Nowadays, most of the propylene is obtained from steam cracking of naphtha, fluid catalytic cracking in the oil refining and natural gas processing (Lazonby, 2023; Agarwal et al., 2018; Cavani et al., 2007). However, the current propylene demand is not satisfied by these technologies and it has been necessary to find other alternatives (Agarwal et al., 2018; The Propylene Gap: How Can It Be Filled - American Chemical Society, 2018; Dong et al., 2021). In this way, a great interest has been aroused in the production of propylene from propane, which is generally easily available and has a relatively low-cost (Brazdil, 2006; Grasselli, 1999; Amghizar et al., 2017).

In fact, propylene production can be obtained by catalytic dehydrogenation (DH) of propane by using catalysts of Pt-Sn or Cr_2O_3 supported on alumina (for Oleflex or Catofin technologies, respectively). However, this method is energetically very unfavorable because it is a strong endothermic process that needs to be performed above 600 °C, presents thermodynamic constraints that limit the propane conversion, as well as it suffers from rapid catalyst deactivation due to coke formation (Cavani et al., 2007; Carrero et al., 2014). Oxidative dehydrogenation (ODH) of propane may be a promising alternative to obtain propylene from propane. This reaction is exothermic and can be performed at lower temperatures (<550 °C) (Dong et al., 2021), it is thermodynamically unrestricted and the catalysts are not usually deactivated by coke deposition (Cavani et al., 2007; Carrero et al., 2014). However, the current values of yield and/or productivity to propylene obtained by propane ODH are still not sufficiently high to be profitable at industrial scale due to the undesirable combustion reactions to CO and CO_2 (CO_x), which are difficult to control (Cavani et al., 2007). Dispersed vanadia species over different supports (ZrO_2, TiO_2, Al_2O_3, SiO_2, CeO_2, etc.) are the most reported catalysts in the propane ODH reaction (Cavani et al., 2007; Carrero et al., 2014; Corma et al., 1992; Singh et al., 2024; Schumacher et al., 2023; Schumacher et al., 2023; Frank et al., 2007; Liu et al., 2002; Liu et al., 2004). In such catalysts, the presence of crystalline phase of vanadium oxide is detrimental for the catalytic activity (Guerrero-Pérez, 2017; Khodakov et al., 1998). Deep analysis of the reaction mechanism, determining the kinetic

* Corresponding author at: Chemical Engineering Department, University of Málaga, Campus Universitario de Teatinos, s/n, E29071, Málaga, Spain.
E-mail address: cordero@uma.es (T. Cordero).

https://doi.org/10.1016/j.ces.2024.120192
Received 8 February 2024; Received in revised form 17 April 2024; Accepted 25 April 2024
Available online 26 April 2024

Nomenclature

Ads_j	Adsorption step represented in Scheme 1
BET	Brunauer, Emmett and Teller
C_i	Surface concentration of *i* species
C_T	Surface concentration of total active sites
DH	Dehydrogenation
$Ea_{App,j}$	Apparent activation energy of *j* reaction step [kJ·mol^{-1}]
Ea_j	Activation energy of *j* reaction step [kJ·mol^{-1}]
EDXA	Energy-dispersive X-ray analyzer
$F_{C3,o}$	Propane inlet molar flow [mol·min^{-1}]
$F_{i,o}$	Inlet molar flow of *i* compound [mol·min^{-1}]
FID	Flame ionization detector
FTIR	Fourier-transform infrared spectroscopy
GC	Gas chromatography
$k_{o,j}$	Preexponential factor of *j* reaction step
$K_{o,j}$	Preexponential factor of *j* adsorption step
$k_{App,o,j}$	Apparent preexponential factor of *j* reaction step
$k_{App,j}$	Apparent rate constant of *j* reaction step
k_j	Rate constant of *j* reaction step
K_j	Equilibrium adsorption constant of *j* step
MK	Mars-van Krevelen
n_i	Number of carbon atoms per molecule of *i* compound
ODH	Oxidative dehydrogenation
P_i	Partial pressure of *i* compound [atm]
$P_{i,o}$	Inlet partial pressure of *i* compound [atm]
$Q_{C3,o}$	Propane inlet volumetric flow [mL·min^{-1}]
Q_T	Total volumetric flow [mL·min^{-1}]
RDS	Rate determining step
r_j	Reaction rate of *j* step [mol·min^{-1}·g^{-1}]
R_j	Reaction step represented in Scheme 1
$S_{exp,i}$	Experimental selectivity to *i* product
$S_{sim,i}$	Simulated selectivity to *i* product
STP	Standard temperature and pressure
TCD	Thermal conductivity detector
TEM	Transmission electron microscopy
TOF	Turnover frequency [s^{-1}]
W_{Cat}	Mass of catalyst [g]
X_{exp}	Experimental propane conversion
X_{sim}	Simulated propane conversion
XPS	X-ray photoelectron spectroscopy
XRD	X-ray diffraction
$Y_{exp,i}$	Experimental yield to *i* product
$Y_{sim,i}$	Simulated yield to *i* product

Greek letters

ΔH_j	Enthalpy of adsorption for *j step* [kJ·mol^{-1}]
θ_i	Fraction of sites or Surface coverage of *i* adsorbed species

parameters, would be a good strategy for improving these catalysts and to optimize the operating conditions in order to increase the yield and productivity to propylene.

In this sense, different kinetics models have been used (Power Law, Langmuir-Hinshelwood, Eley-Rideal, etc. (Frank et al., 2007; Bottino et al., 2003; Argyle et al., 2002; Creaser and Andersson, 1996; Andersson, 1994), but the Mars-van Krevelen (MK) expression (Mars and van Krevelen, 1954) is the most frequently proposed for ODH reactions in the literature (Carrero et al., 2014; Mars and van Krevelen, 1954; Grabowski, 2006; Kondratenko et al., 2005; Dinse et al., 2008; Jibril et al., 2004; Baldi et al., 1998; Routray et al., 2004; Chakraborty et al., 2015). The MK type mechanism considers that the lattice oxygens of the catalyst are responsible for the hydrocarbon oxidation, being these oxygen species the ones that are transferred into the structure of the hydrocarbon molecule to form reaction intermediates and/or products. In the case of propane ODH, the catalyst is reduced by the reaction with propane and is simultaneously reoxidized with gas-phase oxygen or other oxidizing agents as N_2O and CO_2 (Kondratenko et al., 2005; Kondratenko and Baerns, 2001; Balogun et al., 2021; Rogg and Hess, 2021). Most of the reaction networks proposed in the literature usually have in common that the mechanism is a parallel-consecutive reaction pathway, where propane and more probably the produced propylene can be totally oxidized forming CO_x (Grabowski, 2006). However, only a few studies have been found in the literature studying in detail reaction steps involving the total oxidation (Grabowski, 2006). The first hydrogen abstraction from propane is usually considered the rate determining step (RDS), whose activation energy is the most frequently compared kinetic parameter between the different catalysts in the literature (Carrero et al., 2014; Grabowski, 2006). However, a wide range of values can be found, probably due to the variety of different kinetic models used (Carrero et al., 2014; Frank et al., 2007; Khodakov et al., 1998; Bottino et al., 2003; Argyle et al., 2002; Creaser and Andersson, 1996; Andersson, 1994; Grabowski, 2006; Kondratenko et al., 2005; Dinse et al., 2008; Jibril et al., 2004; Baldi et al., 1998; Routray et al., 2004; Chakraborty et al., 2015; Khodakov et al., 1999; Carrero et al., 2014; Zhang and Liu, 2019; Michaels et al., 1996; Dinse et al., 2009), which are sometimes oversimplified and/or frequently inconsistent and without physical relevance.

With this regard, Vannice stated that the rate equation derived from the MK mechanism to describe redox reactions should be only considered as a mathematical fitting function without physical relevance (Vannice, 2007). The major discrepancy is found in the rate of oxygen adsorption, which must have dissociative character in order to form the lattice oxygen that will be responsible for the hydrocarbon oxidation. However, molecular oxygen adsorption in a single site is reflected in MK rate equation. Other inconsistencies come from the consideration of non-elementary steps in the rate equations and the non-inclusion of intermediate species or final products in the site balance, considering only oxygen ions (even though the equation represents molecular oxygen adsorption). Furthermore, many authors have simplified to zero-order dependence the rate equations assuming that the reoxidation reaction of the catalyst is much faster than the reduction reaction (Khodakov et al., 1998; Argyle et al., 2002; Creaser and Andersson, 1996; Khodakov et al., 1999; Carrero et al., 2014; Zhang and Liu, 2019; Michaels et al., 1996; Dinse et al., 2009), and consequently, sometimes, even taking for granted that the catalyst is fully oxidized or nearly saturated with oxygen under reaction conditions (Creaser and Andersson, 1996; Carrero et al., 2014). These assumptions have become generalized and accepted in the literature for this kind of catalysts in ODH reactions, and probably it is right for a broad range of catalysts and operation conditions. However, it is possible that sometimes these assumptions are not true even at low conversions, since it will depend on the catalyst nature and reaction conditions.

Propane TOF is widely used to compare the activity of the catalysts, however different tendencies can be found. For example, it has been reported that as the vanadium content of the catalyst increases, the propane turnover frequency (TOF) decreases (Solsona et al., 203 (2001); Christodoulakis et al., 2004), remains constant (Carrero et al., 2014; Gao et al., 2002; Shee et al., 2006; Rao and Deo, 2007) or increases (Khodakov et al., 1999; Chen et al., 2002; Viparelli et al., 1999). These discrepancies can be related to the use of different synthesis methods, supports and concentrations, which may result in different kind of vanadia surface species. Moreover, it cannot be discarded the possible existence of external and/or internal mass and/or heat transport limitations, as well as contribution of homogenous phase reaction at high

temperatures (above 500 °C) and/or experiments with a total oxygen conversion, thus hindering the determination of the reaction mechanism and the derived kinetic rates and parameters.

In previous works, FTIR and Raman *operando* spectroscopy were combined for the study of vanadium-based catalysts during propane ODH (Ternero-Hidalgo et al., 2020; Ternero-Hidalgo et al., 2021). These experiments allowed the simultaneous characterization of the adsorbed species or reaction intermediates and of the catalyst structure, as well as the measurement of the activity results with both on line mass spectrometry and FTIR spectroscopy. The results obtained were used to establish the possible intermediates and to identify the role of different oxygen species bound to vanadium sites. Then, the propane ODH reaction was evaluated on a vanadium oxide-based submicron diameter fiber catalyst (Ternero-Hidalgo et al., 2018). The use of electrospinning technique allowed the preparation of catalysts with very uniform composition and with submicrometric fibrous structure, which confers small internal diffusion resistance to the catalyst compared to traditional powdered catalysts, as well as less temperature gradients and lower pressure drop when they are packed in a fixed-bed (Reichelt et al., 2014). These advantages made easier the performance of the experiments, without the addition of diluting inert material (e.g. silicon carbide (Pérez-Ramírez et al., 2000; Berger et al., 2002), while isolating the obtention of intrinsic kinetic data of the catalyst without the interference of other effects. The aim of this work is to develop a rigorous kinetic model to predict the surface coverage of the different adsorbed species and the fraction of sites of vanadia species present on the catalyst at certain conditions of temperature, space–time and inlet partial pressures of propane and oxygen, which determines the conversion-selectivity profiles of the catalyst. In this way, a set of reaction experiments in a fixed-bed reactor has been performed to estimate the corresponding kinetic parameters.

2. Materials and methods

2.1. Catalyst preparation and characterization

The vanadium oxide based submicron-fiber catalyst, F-PZr-V5.0, was prepared using the electrospinning technique following the synthesis method previously described (Ternero-Hidalgo et al., 2018). Briefly, a polymer solution prepared with zirconium (IV) propoxide, polyvinylpyrrolidone (PVP), acetylacetone, vanadyl acetylacetonate and 1-propanol was vigorously stirred for 24 h at room temperature. The solution was electrospun using a distance between the needle and the collector of 20 cm, electrical potential difference of 12 kV (the tip at + 6 kV and the collector was at − 6 kV), and a flow rate of 0.5 mL/h. Then, the electrospun fibers were calcined in a conventional tubular furnace with a heating rate of 10 °C/min up to 500 °C, whose temperature was kept for 6 h in air flow (150 mL/min STP) to eliminate the organic part and the remaining solvent, as well as to stabilize the final inorganic zirconia fibers, containing a nominal vanadium mass concentration of 5.0 % (F-PZr-V5.0).

2.2. Propane ODH experiments

The catalyst F-PZr-V5.0 was evaluated for the reaction of propane oxidative dehydrogenation (ODH) in a fixed-bed microreactor (i.d. 4 mm) placed inside a vertical furnace with temperature control (the same than previous works (Ternero-Hidalgo et al., 2018; Ternero-Hidalgo et al., 2018). The reaction temperature was varied from 300 to 400 °C. The feed was prepared by a mixture of three gases: propane (99.95 %), oxygen (99.999 %) and helium (99.999 %). The gases were mixed to obtain different feed compositions by using mass flow controllers, varying both the propane and oxygen inlet partial pressures ($P_{C3,o}$ and $P_{O2,o}$, respectively) from 0.025 to 0.2 atm. The total volumetric gas flow (Q_T) and the mass of catalyst (W_{Cat}) were adjusted in order to vary the space–time ($W_{Cat}/Q_{C3,o}$) in the range of 0.1–1.0 $g_{cat}{\cdot}s{\cdot}mL^{-1}_{C3H8}$ (volume was always expressed in standard temperature and pressure (STP) conditions: 20 °C and 101.325 kPa), which are typical units and range of values used in the literature (Cavani et al., 2007; Carrero et al., 2014). The pipelines were heated at 120 °C to preheat the reactant mixture upstream the reactor and to avoid condensation of products downstream the reactor. Table S1 summarizes the conditions used in the different experiments.

Reactants and products were analyzed in steady state conditions by an on-line gas chromatograph (Perkin-Elmer, Clarus 500 GC), equipped with a Hayesep D 80/100 (length: 3 m; diameter: 1/8″; internal diameter; 2.1 mm) and an active carbon 80/100 (length: 2 m; diameter 1/8″; internal diameter: 2,1 mm) packed columns. Light gases (O_2, CO and CO_2) were detected by a thermal conductivity detector (TCD); C_3H_6 and C_3H_8, and other hydrocarbons if present, were detected using a flame ionization detector (FID). In all the cases carbon and oxygen molar balances were closed with errors lower than 5 %. The propane conversion and the selectivity or yield to *i* product are defined as *X* and S_i or Y_i, respectively:

$$X = \frac{P_{C3,o} - P_{C3}}{P_{C3,o}} \tag{1}$$

$$S_i = \frac{n_i \cdot P_i}{n_{C3} \cdot P_{C3,o} \cdot X} \tag{2}$$

$$Y_i = X \cdot S_i \tag{3}$$

where $P_{C3,o}$ and P_{C3} are the partial pressures of propane in the inlet and in the outlet streams, respectively. P_i is the partial pressure of *i* product in the outlet stream, and n_{C3} or n_i are the number of carbon atoms per molecule of propane ($n_{C3} = 3$) or *i* product, respectively.

Previous studies conducted on a similar catalytic system, confirmed the absence of catalyst deactivation during reaction. As well as a negligible contribution of homogenous phase reaction or participation of zirconia in the observed catalytic activity (Ternero-Hidalgo et al., 2018). Moreover, external mass and heat transport limitations were negligible under the studied conditions, while internal mass and heat transport limitation can be discarded due to the short diffusion pathways in the submicron-fibers (diameter of 300–400 nm). Finally, no significant pressure drop was observed through the catalyst bed under the experimental conditions used owing to the fibrous morphology of the catalyst (Reichelt et al., 2014).

3. Results and discussion

3.1. Catalyst characterization

The surface morphology of the fiber catalyst was studied by transmission electron microscopy (TEM), where fibrous morphology of the catalyst with diameters ranging from 300 to 410 nm was observed. The porous texture was characterized by N_2 adsorption–desorption at −196 °C, obtaining a type IVa isotherm corresponding to mesoporous solid and a BET surface area of 66 $m^2{\cdot}g^{-1}$. The surface chemistry and crystal structure of the sample were analyzed by energy-dispersive X-ray (EDXA), X-ray photoelectron spectroscopy (XPS), in situ Raman and X-ray diffraction patterns (XRD). The results showed the presence of vanadium uniformly distributed along the fibers, being the vanadium mass concentration very close to the nominal value, 5.0 % by both TEM/EDX and XPS analyses. Raman results confirmed the presence of VO_x dispersed species, along the tetragonal zirconia, in form of monovanadate and polyvanadate species. Moreover, vanadium crystal structures as V_2O_5 or ZrV_2O_7 were not detected for this sample. Fig. 1 and Table 1 summarize all the physicochemical characteristics above mentioned. A detailed characterization of the sample F-PZr-V5.0 was already reported in a previous work (Ternero-Hidalgo et al., 2018).

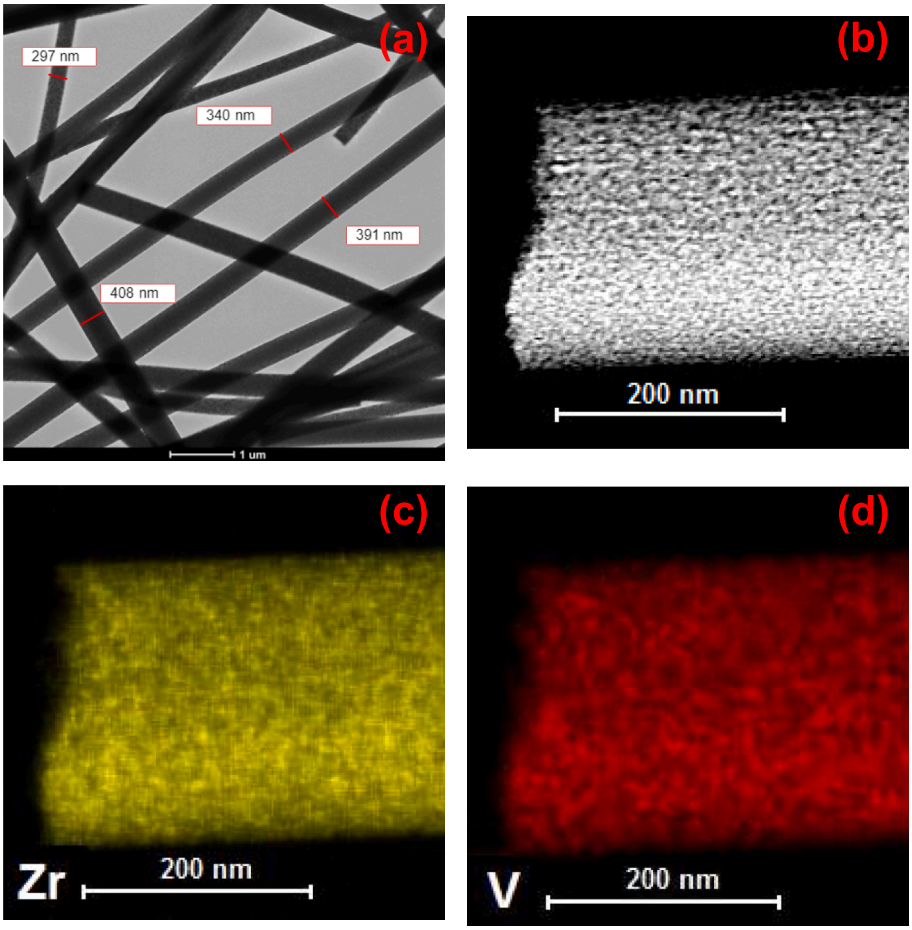

Fig. 1. TEM (a) and HAADF-STEM (b) micrographs, and EDX elemental mappings of Zr (c) and V (d) for the sample F-PZr-V5.0.

Table 1
Summary of the physicochemical characteristics of F-PZr-V5.0.

Property	Analysis Method	Result
Surface morphology	TEM	Submicron fibers with diameters of 300–410 nm
BET surface area	Adsorption–desorption of N_2 at −196 °C	66 $m^2 \cdot g^{-1}$
Surface chemistry and crystal structure	TEM/EDX	4.7 wt% V
	XPS	4.9 wt% V2p
	Raman	VO_x dispersed species (monovanadates and polyvanadates) and tetragonal ZrO_2
	XRD	Tetragonal ZrO_2

3.2. Propane ODH mechanism

Scheme 1 represents the detailed mechanism proposed in a previous work from the FTIR-Raman *operando* results for a similar catalyst (Ternero-Hidalgo et al., 2021), where it is assumed the mediation of lattice oxygen in the ODH reaction. This lattice oxygen can react with propane in gas phase and the rest of adsorbed species involved in the reaction. Simultaneously, the gas-phase oxygen reoxidizes the vanadium sites from the VO_x lattice that are being reduced during the above reactions. This latter reaction step is necessary to continue the catalytic cycle. Note that lattice oxygens in the form of V-O-V or V-O-Zr groups have been represented in the same way, as (V-O), and it has been assumed that both have the same role in the mechanism, although it is possible that they present slightly different activity. The participation of V = O terminal groups in the reaction mechanism is discarded, since it seemed to be much less active than V-O sites. (V-OH) and (V-□) represent a protonated lattice oxygen and a vacant site, respectively.

The reoxidation reactions of the catalyst are represented by the equations R_{O2} and $R_{V\text{-}OH}$ (Eqs. (4) and (5), respectively), which describe the irreversible dissociative adsorption of O_2 from the gas phase and the reversible recombination of V-OH forming H_2O, V-O and V-□ sites, respectively. On the other hand, it is proposed that propane is firstly activated forming the corresponding isopropoxide (R_{C3}; Eq. (6)), which can evolve as propylene (Eqs. (7) and (8)) or can be further oxidized to chemisorbed acetone ($R_{Acetone}$; (Eq. (9)). Propylene can adsorb again on a V-O site of the catalyst ($Ads_{C3=}$, (Eq. (8)) and react with a neighbour V-OH, which is a Brønsted acidic site, forming isopropoxide ($R_{C3=}$; Eq. (7)), to finally continue with the subsequent oxidation steps. Then, oxidative cleavage of the C(1)-C(2) bond of chemisorbed acetone gives rise to the formation of bidentate formates and acetates ($R_{Carboxylate}$; (Eq. (10)). Afterwards, these carboxylates species evolve as CO in the gas phase ($R_{Formate}$ and $R_{Acetate}$; Eqs. (11) and (12)). It should be noted that, unlike the formate species, acetate species require lattice oxygen to decompose. Finally, CO can be further oxidized to CO_2 and desorb (R_{CO2}; Eq. (13)). The oxidation of formates, acetates and CO through the formation of carbonates species has not been represented in the scheme. Although this oxidation cannot be totally discarded (Baldi et al., 1998; Busca et al., 1999; Finocchio et al., 1994), their contribution to the

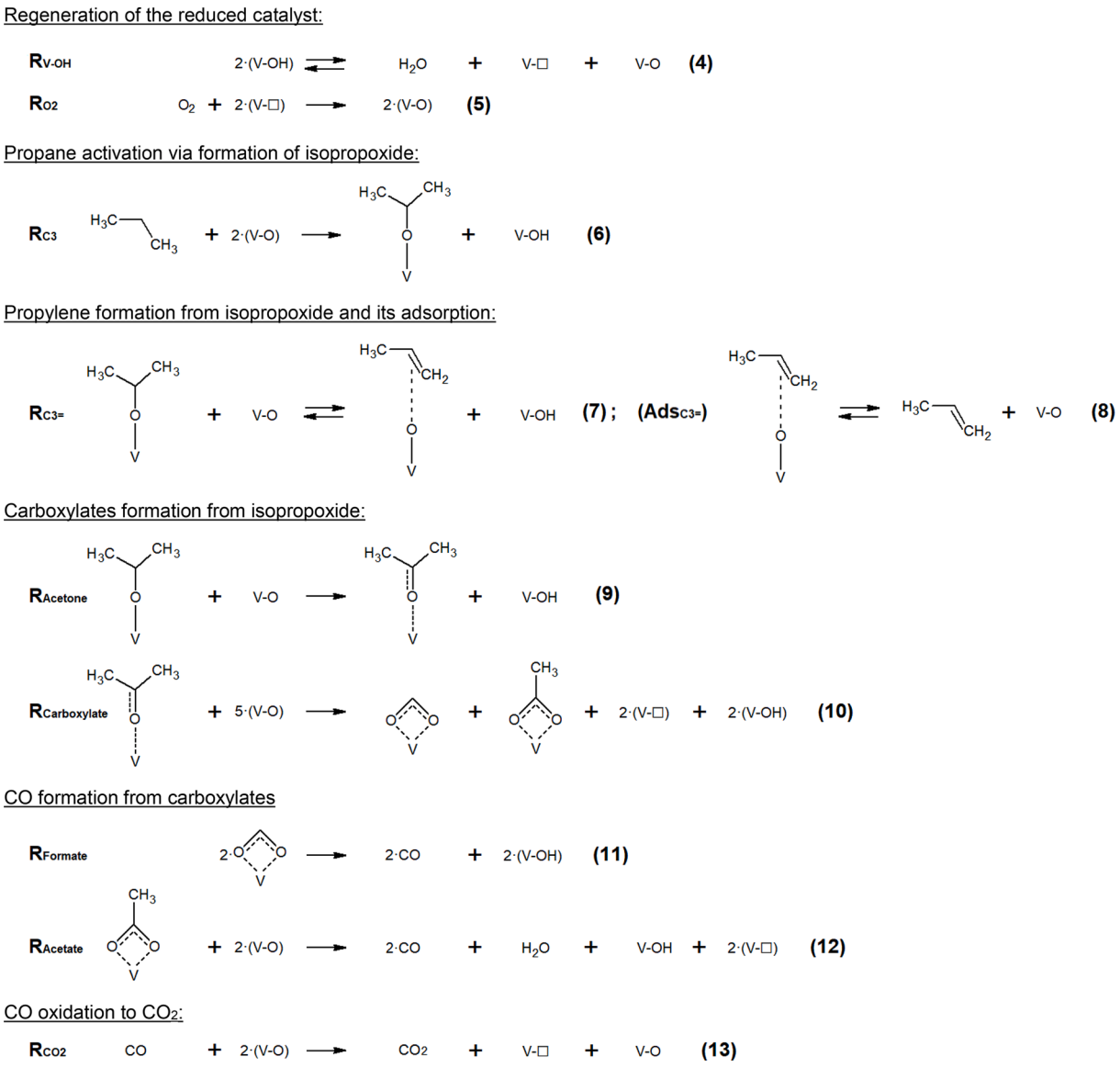

Scheme 1. Proposed detailed mechanism of the propane ODH.
adapted from Ternero-Hidalgo et al., 2021

kinetic rate is likely to be minimal in the current range of studied operation conditions.

3.3. Kinetic study

The kinetic equations will be derived from the proposed reaction mechanism (Eqs. (4)–(13)) shown in Scheme 1. The site balance would be as follows:

$$C_T = C_{V-O} + C_{V-OH} + C_{V-\square} + C_{Acetate} + C_{Formate} \quad (14)$$

where C_T is the total concentration of surface sites and C_i the surface concentration of *i* sites or adsorbed i species. The surface concentrations of isopropoxide, adsorbed propylene and chemisorbed acetone have not been included, since they are negligible with respect to the other species, as it was already observed in the operando spectroscopic results (Ternero-Hidalgo et al., 2021). Alternatively, if Eq. (14) is divided by C_T, it can be rewritten as a function of fraction of sites and surface coverages of adsorbed species:

$$1 = \theta_{V-O} + \theta_{V-OH} + \theta_{V-\square} + \theta_{Acetate} + \theta_{Formate} \quad (15)$$

where θ_i is the fraction of *i* sites or surface coverages of *i* adsorbed species. It should be noted that the rate equations will be expressed as a function of fraction of sites and surface coverages, then, the rate constants will include C_T combined with the preexponential factors, being $k_i = C_T \cdot k'_i$, resulting in a first-order dependence on C_T for all the cases, where k'_i contains the probability factor for nearest-neighbor (Vannice, 2005).

Since surface oxidation reactions in redox mechanism usually consist of sequences of irreversible steps in nature, it will be assumed that all the steps are irreversible (Vannice, 2007), except the ones related to the propylene formation and adsorption (Eqs. (7) and (8), respectively). The dehydration surface reaction (Eq. (4)) necessary for the catalyst reoxidation, which has been reported to be reversible (Chen et al., 2000; Chen et al., 1999); it has been also considered as irreversible reaction due to the fast full reoxidation of the catalyst, observed in previous studies (Ternero-Hidalgo et al., 2020; Ternero-Hidalgo et al., 2021). The reactions of adsorbed formate species oxidation and CO_2 formation (Eqs. (11) and (13)) are considered second order with respect to the surface coverages of formate and fraction of active sites (V-O), respectively, assuming that carbonates species are formed as surface intermediates in

Table 2
Proposed kinetic equations for the reaction mechanism detailed in Scheme 1.

REACTION MECHANISM	PROPOSED KINETIC EQUATION
Regeneration of the reduced catalyst	
$R_{V\text{-}OH}$ (4)	$r_{V-OH} = -k_{V-OH}\cdot\theta_{V-OH}^2$ (16)
R_{O2} (5)	$r_{O2} = -k_{O2}\cdot P_{O2}\cdot\theta_{V-\square}^2$ (17)
Propane activation via formation of isopropoxide	
R_{C3} (6)	$r_{C3} = -k_{C3}\cdot P_{C3}\cdot\theta_{V-O}^2$ (18)
Propylene formation from isopropoxide and its adsorption	
$R_{C3=}$ & $Ads_{C3=}$ (7) & (8)	$r_{C3=} = k_{\underset{C3=}{\rightarrow}}\cdot\theta_{Isopropoxide}\cdot\theta_{V-O} - k_{\underset{C3=}{\leftarrow}}\cdot\theta_{V-O-C3=}\cdot\theta_{V-OH}$ (19)
Carboxylates formation from isopropoxide	
$R_{Acetone}$ (9)	$r_{Acetone} = k_{Acetone}\cdot\theta_{Isopropoxide}\cdot\theta_{V-O}$ (20)
CO formation from carboxylates	
$R_{Formate}$ (11)	$r_{Formate} = -k_{Formate}\cdot\theta_{Formate}^2$ (21)
$R_{Acetate}$ (12)	$r_{Acetate} = -k_{Acetate}\cdot\theta_{Acetate}\cdot\theta_{V-O}^2$ (22)
CO oxidation to CO_2	
R_{CO2} (13)	$r_{CO2} = k_{CO2}\cdot P_{CO}\cdot\theta_{V-O}^2$ (23)

such reactions. The reaction of adsorbed carboxylates species formation (Eq. (10)), as expressed in Scheme 1, is a multi-body interaction, which is very improbable that happens as an elementary step. Nevertheless, it is not kinetically significant or necessary in the development of the kinetic model, therefore it has not been taken into account. According to the above assumptions, the reaction rates (Eqs. (16)–(23)) for the Eqs. (4)–(13) are summarized in Table 2, where in Eqs. (16) and (17), r_{V-OH} and r_{O2} are the consumption rates of V-OH sites and molecular oxygen to reoxidize the catalyst, respectively, being k_{V-OH} and k_{O2} their respective rate constants; and P_{O2} is the oxygen partial pressure. r_{C3}, in Eq. (18), is the rate of propane consumption, being k_{C3} its rate constant and P_{C3} is the propane partial pressure. In Eq. (19), $r_{C3=}$ is the rate of the reversible reaction of propylene formation on the V-O site, where $k_{\underset{C3=}{\rightarrow}}$ and $k_{\underset{C3=}{\leftarrow}}$ represent the forward and reverse rate constants, respectively; and $\theta_{Isopropoxide}$ and $\theta_{V-O-C3=}$ are the surface coverages of isopropoxide and adsorbed propylene, respectively. $r_{Acetone}$, $r_{Formate}$ and $r_{Acetate}$, in Eqs. (20), (21) and (22), are the formation rate of chemisorbed acetone, and the decomposition rates of formate and acetate species, respectively; being $k_{Acetone}$, $k_{Formate}$ and $k_{Acetate}$ their respective rate constants. In Eq. (23), r_{CO2} is the formation rate of CO_2 from oxidation of CO, being k_{CO2} its rate constant and P_{CO} the CO partial pressure. Finally, the formation rate of CO can be derived from making a balance between the CO formed by the evolution of formate and acetate species, and the CO consumed in its oxidation to form CO_2:

$$r_{CO} = -r_{Formate} - 2\cdot r_{Acetate} - r_{CO2} \tag{24}$$

Among all the species involved in the proposed reaction mechanism (Scheme 1), propane is the most stable towards the oxidation. Therefore, it will be considered that the propane activation reaction, via first hydrogen abstraction from propane (Eqs. (6) and (18)), is the rate-determining step (RDS) as reported elsewhere (Grabowski, 2006). This means that Eq. (18) will determine the overall rate of the catalytic cycle and, therefore, also the propane conversion. In addition, it will be assumed that the propylene adsorption step (Eq. (8)) is in steady state. This assumption will only be valid if both the forward and reverse adsorption rates are several orders of magnitude greater than the RDS, which is reasonable in this case. In this way, it could be possible to express the Eq. (19) as a function of propylene partial pressure, $P_{C3=}$, which can be measured during reaction, instead of surface coverage of adsorbed propylene, $\theta_{V-O-C3=}$, which is very difficult to quantify from experiment. Therefore, if the adsorption equilibrium constant of propylene is considered as:

$$K_{Ads,C3=} = \frac{\theta_{V-O-C3=}}{P_{C3=}\cdot\theta_{V-O}} \tag{25}$$

and

$$k_{App,\underset{C3=}{\leftarrow}} = K_{Ads,C3=}\cdot k_{\underset{C3=}{\leftarrow}} \tag{26}$$

where $k_{App,\underset{C3=}{\leftarrow}}$ is an apparent reaction rate constant that combines the equilibrium constant of propylene adsorption, $K_{Ads,C3=}$, and the reverse rate constant of the reversible reaction of adsorbed propylene formation, $k_{\underset{C3=}{\leftarrow}}$. Then, Eq. (19) can now be rewritten as follows:

$$r_{C3=} = k_{\underset{C3=}{\rightarrow}}\cdot\theta_{Isopropoxide}\cdot\theta_{V-O} - k_{App,\underset{C3=}{\leftarrow}}\cdot P_{C3=}\cdot\theta_{V-O}\cdot\theta_{V-OH} \tag{27}$$

Moreover, as the catalyst is supposed to operate at steady-state conditions, then:

$$r_{C3} + r_{C3=} + r_{Acetone} = 0 \tag{28}$$

$$r_{Acetone} = r_{Carboxylate} = r_{Formate} = r_{Acetate} = \frac{r_{CO} + r_{CO2}}{3} \tag{29}$$

and

$$r_{C3} = -r_{C3=} - \frac{r_{CO} + r_{CO2}}{3} \tag{30}$$

where $r_{Carboxylate}$ is the formation rate of carboxylates from chemisorbed acetone (Eq. (10)), and r_{CO} and r_{CO2} are divided by 3 due to stoichiometric relationships. Eqs. (28) and (29) indicate that all the isopropoxide formed from the converted propane will be consumed by two parallel reactions; on one hand, forming adsorbed propylene that will evolve as propylene; and on the other hand, forming chemisorbed acetone that will yield as CO, which can also be further oxidized to CO_2 (Eq. (30)). Therefore, the ratio among both parallel reactions for a given conditions will determine the selectivity to propylene and to CO_x. It is interesting to note that the rate constants belonging to Eq. (19) ($r_{C3=}$) and Eq. (20) ($r_{Acetone}$) must be several orders of magnitude greater than the ones belonging to the RDS, in this case Eq. (18) (r_{C3}), as above mentioned.

Making balance and assuming pseudo-steady state for each adsorbed species and site, the rate of change of their respective surface coverages or fraction of sites should be approximately zero:

$$\frac{d\theta_{Isopropoxide}}{dt} = -r_{C3} - r_{C3=} - r_{Acetone} \approx 0 \tag{31}$$

$$\frac{d\theta_{Formate}}{dt} = r_{Carboxylate} - r_{Formate} \approx 0 \tag{32}$$

$$\frac{d\theta_{Acetate}}{dt} = r_{Carboxylate} - r_{Acetate} \approx 0 \tag{33}$$

$$\frac{d\theta_{V-OH}}{dt} = -r_{C3} + r_{C3=} + r_{Acetone} + 2\cdot r_{Carboxylate} - r_{Formate} - r_{Acetate} - r_{V-OH} \approx 0 \tag{34}$$

$$\frac{d\theta_{V-\square}}{dt} = 2\cdot r_{Carboxylate} - 2\cdot r_{Acetate} + r_{CO2} - \frac{r_{V-OH}}{2} + 2\cdot r_{O2} \approx 0 \tag{35}$$

$$\frac{d\theta_{V-O}}{dt} = -2\cdot r_{O2} - \frac{r_{V-OH}}{2} + 2\cdot r_{C3} - r_{Acetone} - 5\cdot r_{Carboxylate} + 2\cdot r_{Acetate} - r_{CO2} \approx 0 \tag{36}$$

Using equations (Eqs. (31)–(36)) and taking into consideration the Eqs. (28) and (29) deduced from steady-state approximations, together with Eqs. (16)–(24) and (27) above proposed as rate expressions, it is possible to deduce the equations for the surface coverages of isopropoxide, formate and acetate adsorbed species, as well as the fraction of V-OH and V-□ sites (Eqs. (37)–(41), respectively).

$$\theta_{Isopropoxide} = \frac{k_{C3}\cdot P_{C3} + k_{App,\underset{C3=}{\leftarrow}}\cdot P_{C3=}\cdot\left(\frac{\theta_{V-OH}}{\theta_{V-O}}\right)}{k_{\underset{C3=}{\rightarrow}} + k_{Acetone}}\cdot\theta_{V-O} \quad (37)$$

$$\theta_{Formate} = \sqrt{\frac{k_{Acetone}}{k_{Formate}}\cdot\theta_{Isopropoxide}}\cdot\theta_{V-O} \quad (38)$$

$$\theta_{Acetate} = \frac{k_{Acetone}}{k_{Acetate}}\cdot\theta_{Isopropoxide} \quad (39)$$

$$\theta_{V-OH} = \sqrt{\left(\frac{2\cdot k_{C3}}{k_{V-OH}\cdot\left(k_{\underset{C3=}{\rightarrow}} + k_{Acetone}\right)}\right)\cdot\left(\left(k_{\underset{C3=}{\rightarrow}} + 3\cdot k_{Acetone}\right)\cdot P_{C3} + 2\cdot k_{Acetone}\cdot k_{App,\underset{C3=}{\leftarrow}}\cdot P_{C3=}\cdot\left(\frac{\theta_{V-OH}}{\theta_{V-O}}\right)\right)}\cdot\theta_{V-O} \quad (40)$$

$$\theta_{V-OH} = \sqrt{\frac{2\cdot k_{C3}\cdot\left(k_{\underset{C3=}{\rightarrow}} + 3\cdot k_{Acetone}\right)}{k_{V-OH}\cdot\left(k_{\underset{C3=}{\rightarrow}} + k_{Acetone}\right)}\cdot P_{C3}}\cdot\theta_{V-O} \quad (41)$$

$$\theta_{V-\square} = \sqrt{\frac{k_{C3}\cdot P_{C3}\cdot\left(k_{\underset{C3=}{\rightarrow}} + 7\cdot k_{Acetone}\right) + 4\cdot k_{Acetone}\cdot k_{App,\underset{C3=}{\leftarrow}}\cdot P_{C3=}\cdot\left(\frac{\theta_{V-OH}}{\theta_{V-O}}\right) + \left(k_{\underset{C3=}{\rightarrow}} + k_{Acetone}\right)k_{CO2}\cdot P_{CO}}{2\cdot k_{O2}\cdot P_{O2}\cdot\left(k_{\underset{C3=}{\rightarrow}} + k_{Acetone}\right)}}\cdot\theta_{V-O} \quad (42)$$

It should be noted that the term $2\cdot k_{Acetone}\cdot k_{App,\underset{C3=}{\leftarrow}}\cdot P_{C3=}\cdot\left(\frac{\theta_{V-OH}}{\theta_{V-O}}\right)$ has been neglected versus the term $\left(k_{\underset{C3=}{\rightarrow}} + 3\cdot k_{Acetone}\right)\cdot P_{C3}$ in (Eq. (40), when handling the balance of Eq. (34) to get the expression for the fraction of sites in form of V-OH (Eq. (41)). $k_{\underset{C3=}{\rightarrow}}$ is related to the second hydrogen abstraction from isopropoxide to form propylene and it should be significantly larger than the other kinetic constants, resulting a surface coverage of isopropoxide species on the catalyst negligible in most of the reaction conditions. This simplification allows to obtain much simpler equations for the fraction of V-OH sites, and subsequently also for V-O sites. The site balance equation (Eq. (15)) can be combined with equations (Eqs. (37)–(39), (41) and (42)) and rearranged for delivering an expression for θ_{V-O}:

$$\theta_{V-O} = \frac{1 - \frac{k_{Acetone}\cdot\left(k_{C3}\cdot P_{C3} + k_{App,\underset{C3=}{\leftarrow}}\cdot P_{C3=}\cdot\left(\frac{\theta_{V-OH}}{\theta_{V-O}}\right)\right)}{k_{Acetate}\cdot\left(k_{\underset{C3=}{\rightarrow}} + k_{Acetone}\right)}}{1 + \left(\frac{\theta_{V-OH}}{\theta_{V-O}}\right) + \sqrt{\frac{k_{C3}\cdot P_{C3}\cdot\left(k_{\underset{C3=}{\rightarrow}} + 7\cdot k_{Acetone}\right) + 4\cdot k_{Acetone}\cdot k_{App,\underset{C3=}{\leftarrow}}\cdot P_{C3=}\cdot\left(\frac{\theta_{V-OH}}{\theta_{V-O}}\right) + \left(k_{\underset{C3=}{\rightarrow}} + k_{Acetone}\right)k_{CO2}\cdot P_{CO}}{2\cdot k_{O2}\cdot P_{O2}\cdot\left(k_{\underset{C3=}{\rightarrow}} + k_{Acetone}\right)}} + \sqrt{\frac{k_{Acetone}\cdot\left(k_{C3}\cdot P_{C3} + k_{App,\underset{C3=}{\leftarrow}}\cdot P_{C3=}\cdot\left(\frac{\theta_{V-OH}}{\theta_{V-O}}\right)\right)}{k_{Formate}\cdot\left(k_{\underset{C3=}{\rightarrow}} + k_{Acetone}\right)}}} \quad (43)$$

where, according to the Eq. (41):

$$\left(\frac{\theta_{V-OH}}{\theta_{V-O}}\right) = \sqrt{\frac{2\cdot k_{C3}\cdot\left(k_{\underset{C3=}{\rightarrow}} + 3\cdot k_{Acetone}\right)}{k_{V-OH}\cdot\left(k_{\underset{C3=}{\rightarrow}} + k_{Acetone}\right)}\cdot P_{C3}} \quad (44)$$

Then, Eq. (44) can be substituted in Eq. (43) to get the equation of θ_{V-O} as a function of only rate constants and partial pressures (P_{C3}, $P_{C3=}$, P_{CO} and P_{O2}). In this way, it is possible to estimate the surface coverage of all the surface species for a given set of rate constants and partial pressures.

It should be noted that the influence of the partial pressures and/or of the kinetic parameters in the Eqs. (37)–(43) for steady-state conditions is consistent with the experimental observations. For example, when the partial pressures of propane, propylene and CO are zero at any oxygen concentration, the surface coverage for V-O is one (Eq. (43)), meanwhile the fraction of sites or surface coverage of the other species are zero, which would mean that the catalyst is in its highest oxidation state. If the oxygen partial pressure is zero, at any propane, propylene and CO concentrations, the surface coverage for V-O (Eq. (43)) would be zero with V-□ sites as the majority species (Eq. (42)). These experimental conditions make the catalyst be in a deep reduced state as observed in the previous work (Ternero-Hidalgo et al., 2020; Ternero-Hidalgo et al., 2021). In general, as the partial pressure of propane increases and/or of oxygen decreases at a constant temperature, the surface coverage of all the surface species and the fraction of V-OH sites increase (Eqs. (37)–(42)), while the fraction of V-O sites (Eq. (43)) decreases. The same effect occurs when propane conversion increases, as it can be deduced from how propylene and CO partial pressures contributes to the different expressions (Eqs (37)–(43)).

With regard to the influence of the kinetic parameters, Eq. (37) predicts that $\theta_{Isopropoxide}$ should be very small, since $k_{\underset{C3=}{\rightarrow}}$ and $k_{Acetone}$ are necessary to be several orders of magnitude greater than k_{C3} as above mentioned, according to the assumption of r_{C3} as the RDS. This is

consistent with the experimental spectroscopic evidences observed in a previous work, where isopropoxide species were negligible or not detected in most of the reaction conditions (Ternero-Hidalgo et al., 2021). In addition, Eqs. (38) and (39) predict that $k_{Formate}$ and $k_{Acetate}$ should be significantly smaller than $k_{Acetone}$ if the surface coverage of formate and acetate are present in appreciable concentrations, as spectroscopically observed in previous work (Ternero-Hidalgo et al., 2020; Ternero-Hidalgo et al., 2021), otherwise these surfaces species would be in negligible concentrations as isopropoxide. Finally, these *operando* experiments also revealed that lattice oxygen (θ_{V-O}) was the most abundant species under reaction conditions, except in the absence of oxygen. Consequently, k_{V-OH} and k_{O2} should take a value large enough to minimize θ_{V-OH} and $\theta_{V-\square}$ (reduced vanadia species), respectively, so that both of them are forced to be significantly smaller than θ_{V-O} (oxidized vanadia species) for most reaction conditions (Eqs. (41) and (42)).

The necessary experimental data to validate the proposed model and determine the kinetic parameters of each rate equation have been obtained by performing reaction experiments in a fixed-bed reactor. Balance equations of fixed-bed reactor have been used for the interpretation of the experimental data, assuming the following requirements: i) uniform distribution of active sites on the catalyst surface (as shown by the characterization data); ii) axial dispersion and wall effects were discarded since the diameter of the fibers (submicron size) were several orders smaller than the length and diameter of the fixed-bed reactor, respectively; iii) the reactor operated at steady-state conditions; iv) diffusional constraints and transport limitations were discarded v) changes in temperature and pressure within the reactor were neglected. When these conditions are met, the balance equation for the fixed-bed reactor can be simplified obtaining the expression for the ideal plug-flow reactor (Eq. (29)):

$$\frac{1}{P_{C3,o}}\cdot dP_i = r_i \cdot d\left(\frac{W_{Cat}}{F_{C3,o}}\right) \tag{45}$$

where the space–time is expressed as $W_{Cat}/F_{C3,o}$ (ratio between catalyst weight and the inlet propane molar flow). Thus, combining the balance equation (Eq. (45)) of oxygen, propane, propylene, carbon monoxide or carbon dioxide, with their respective rate equation (Eqs. (17), (18), (27), (24) and (23)) and the corresponding surface coverage expressions (Eqs. (37)–(39) and (41)–(43)), the following system of differential equations is obtained:

$$\frac{1}{P_{C3,o}}\cdot\frac{dP_{O2}}{d\left(\frac{W_{Cat}}{F_{C3,o}}\right)} = -k_{O2}\cdot P_{O2}\cdot\theta_{V-\square}^2 \tag{46}$$

$$\frac{1}{P_{C3,o}}\cdot\frac{dP_{C3}}{d\left(\frac{W_{Cat}}{F_{C3,o}}\right)} = -k_{C3}\cdot P_{C3}\cdot\theta_{V-O}^2 \tag{47}$$

$$\frac{1}{P_{C3,o}}\cdot\frac{dP_{C3=}}{d\left(\frac{W_{Cat}}{F_{C3,o}}\right)} = \frac{k_{\underset{C3=}{\rightarrow}}}{k_{\underset{C3=}{\rightarrow}}+k_{Acetone}}\cdot\left(k_{C3}\cdot P_{C3} - \frac{k_{Acetone}}{k_{\underset{C3=}{\rightarrow}}}\cdot k_{App,\underset{C3=}{\leftarrow}}\cdot P_{C3=}\cdot\left(\frac{\theta_{V-OH}}{\theta_{V-O}}\right)\right)\cdot\theta_{V-O}^2 \tag{48}$$

$$\frac{1}{P_{C3,o}}\cdot\frac{dP_{CO}}{d\left(\frac{W_{Cat}}{F_{C3,o}}\right)} = \frac{3\cdot k_{Acetone}}{k_{\underset{C3=}{\rightarrow}}+k_{Acetone}}\cdot\left(k_{C3}\cdot P_{C3}+k_{App,\underset{C3=}{\leftarrow}}\cdot P_{C3=}\cdot\left(\frac{\theta_{V-OH}}{\theta_{V-O}}\right)\right)\cdot\theta_{V-O}^2 - k_{CO2}\cdot P_{CO}\cdot\theta_{V-O}^2 \tag{49}$$

$$\frac{1}{P_{C3,o}}\cdot\frac{dP_{CO2}}{d\left(\frac{W_{Cat}}{F_{C3,o}}\right)} = k_{CO2}\cdot P_{CO}\cdot\theta_{V-O}^2 \tag{50}$$

It has been considered that the dependence of the kinetic and thermodynamic parameters with the temperature follows the Arrhenius law for the kinetic constants and Van't Hoff law for the equilibrium constants.

Integral packed fixed-bed reactor behaviour was considered using the balance Eqs. (46)–(50) for the interpretation of the experimental data. This system of differential equations was numerically solved by a modified Runge-Kutta method, for the proposed kinetic parameters, to calculate the exit partial pressure of each reactant/product, as well as the surface coverage of each adsorbed species participating in the reaction mechanism. Then, the values of propane conversion, selectivity and yield to propylene, CO and CO_2 were calculated by using the partial pressures before obtained and Eqs. (1)–(3). The kinetic parameters were estimated with an optimization routine based on the Levenberg-Marquardt algorithm implemented in Matlab R2016b software to minimize the *error* function:

$$error = \sum_m \left(\sqrt{\left(P_{exp,C3=,m}-P_{sim,C3=,m}\right)^2}+\sqrt{\left(P_{exp,CO,m}-P_{sim,CO,m}\right)^2}+\sqrt{\left(P_{exp,CO2,m}-P_{sim,CO2,m}\right)^2}\right) \tag{51}$$

where $P_{exp,i,m}$ and $P_{sim,i,m}$ are the experimental and simulated partial pressures, respectively, to the compound i for the experiment m. The optimization involved the obtention of the Arrhenius and Van't Hoff parameters, and these kinetic parameters were used to simulate the conversion, selectivity and yield values (Eqs. (1)–(3)) at different space-times, inlet partial pressures of propane and oxygen and reaction temperatures.

Selectivity to propylene will be determined by the ratio $k_{\underset{C3=}{\rightarrow}}/k_{Acetone}$, which only depends on the temperature, together with the propylene adsorption term $k_{App,\underset{C3=}{\leftarrow}}\cdot P_{C3=}\cdot\left(\frac{\theta_{V-OH}}{\theta_{V-O}}\right)$, which is influenced by the temperature as well as the propylene partial pressure (i.e. the conversion) and the ratio of the surface coverages of V-O and V-OH sites, from Eqs. (48) and (49). Therefore, the maximum selectivity to propylene at a determined temperature will be obtained at low conversion values where $P_{C3=}\approx 0$, and it will correspond with the value of $k_{\underset{C3=}{\rightarrow}}/(k_{\underset{C3=}{\rightarrow}}+k_{Acetone})$. It is important to highlight that if the propylene adsorption step is neglected or not taken into consideration in the reaction mechanism (i.e. $k_{App,\underset{C3=}{\leftarrow}}\approx 0$ in Eqs. (48) and (49)), the selectivity to propylene would always reach the above maximum value, which would remain constant with the space–time and without any dependence on the propane conversion. However, according to the results obtained in the previous works (Ternero-Hidalgo et al., 2018; Ternero-Hidalgo et al., 2018) and those found in the literature about propane ODH (Cavani et al., 2007; Carrero et al., 2014; Grabowski, 2006), propane conversion clearly has a great repercussion in the selectivity values, decreasing the one to propylene as the conversion is higher. This is the most important drawback of this reaction, because it makes difficult to obtain high yields to propylene (Cavani et al., 2007). Then, it seems necessary to consider that propylene adsorption presents an important contribution to the reaction mechanism of propane ODH. In fact, it has been reported elsewhere (Carrero et al., 2014; Grabowski, 2006; Dinse et al., 2009) that the majority of detected CO_x come from the combustion of the propylene previously formed, while direct propane combustion is usually neglected. This means that $k_{\underset{C3=}{\rightarrow}}/k_{Acetone}$ should be very high in these cases.

Table 3 summarizes the *error* function value, and the values obtained of preexponential factors and activation energies for all the reaction steps implied in the propane ODH reaction mechanism, whereas Fig. 2

Table 3
Estimated kinetic parameters for the propane ODH reaction of the catalyst studied (F-PZr-V5.0), the 95 % confidence intervals for each estimated parameter were calculated using the MATLAB functions "lsqnonlin" and "nlparci". The ***error*** function values were calculated using Eq. (51) for each of the adjusted variables (propane, CO and CO_2). The kinetic constants evaluated at 350 °C are also shown.

	$k_{o,j}$[a,b,c,d] ($mol \cdot min^{-1} \cdot g^{-1}$)	95 %CI	Ea_j ($kJ \cdot mol^{-1}$)	95 %CI	$k_{o,j}$[a,b,c,d] ($mol \cdot min^{-1} \cdot g^{-1}$) at 350 °C
k_{V-OH}	$1.23 \cdot 10^{10}$	$\pm 2.55 \cdot 10^{5}$	94	± 4.73	$1.79 \cdot 10^{2}$
k_{O2}	[a]$1.72 \cdot 10^{7}$	$\pm 4.31 \cdot 10^{4}$	98	± 10.39	[a]$1.07 \cdot 10^{-1}$
k_{C3}	[b]$2.01 \cdot 10^{6}$	$\pm 5.28 \cdot 10^{3}$	104	± 5.16	[b]$3.76 \cdot 10^{-3}$
$k_{\underset{C3=}{\rightarrow}}$	$1.39 \cdot 10^{15}$	$\pm 2.78 \cdot 10^{10}$	91	± 2.83	$3.11 \cdot 10^{7}$
$k_{App,\underset{C3=}{\leftarrow}}$	[c]$3.64 \cdot 10^{14}$	$\pm 4.72 \cdot 10^{9}$	112	± 2.58	[c]$1.49 \cdot 10^{5}$
$k_{Acetone}$	$1.10 \cdot 10^{11}$	$\pm 2.23 \cdot 10^{6}$	86	± 3.00	$6.666 \cdot 10^{3}$
$k_{Formate}$	$9.78 \cdot 10^{11}$	$\pm 6.37 \cdot 10^{6}$	140	± 9.44	1.66
$k_{Acetate}$	$2.28 \cdot 10^{13}$	$\pm 2.55 \cdot 10^{5}$	181	± 8.35	$1.69 \cdot 10^{-2}$
k_{CO2}	[d]$1.13 \cdot 10^{8}$	$\pm 8.22 \cdot 10^{3}$	116	± 9.62	[d]$2.27 \cdot 10^{-2}$
	error				
C_3H_8	0.016				
CO	0.024				
CO_2	0.016				
Total	0.056				

[a] $(mol \cdot min^{-1} \cdot g^{-1} \cdot atm^{-1}_{O2})$.
[b] $(mol \cdot min^{-1} \cdot g^{-1} \cdot atm^{-1}_{C3H8})$.
[c] $(mol \cdot min^{-1} \cdot g^{-1} \cdot atm^{-1}_{C3H6})$.
[d] $(mol \cdot min^{-1} \cdot g^{-1} \cdot atm^{-1}_{CO})$.

represents the simulated values of propane conversion, selectivity and yield to compound i (X_{sim}, $S_{sim,i}$ and $Y_{sim,i}$, respectively) versus the ones experimentally obtained (X_{exp}, $S_{exp,i}$ and $Y_{exp,i}$, respectively) for these estimated kinetic parameters. The results show that the simulated values predict very well the experimental data, with an *error* function (Eq. (51)) value of 0.056, which seems to validate the mathematical model equations presented in this study, as well as the reaction mechanism previously proposed (Ternero-Hidalgo et al., 2021).

It should be reminded that $k_{App,\underset{C3=}{\leftarrow}}$ is the product between $k_{\underset{C3=}{\leftarrow}}$ and $K_{Ads,C3=}$ (Eq. (26)), which are constants of reaction and adsorption steps, respectively. Then:

$$k_{App,o,\underset{C3=}{\leftarrow}} = k_{o,\underset{C3=}{\leftarrow}} \cdot K_{Ads,o,C3=} \tag{52}$$

$$Ea_{App,\underset{C3=}{\leftarrow}} = Ea_{\underset{C3=}{\leftarrow}} + \Delta H_{Ads,C3=} \tag{53}$$

Considering a propylene adsorption enthalpy on vanadia species $(\Delta H_{Ads,C3=})$ of around −40 $kJ \cdot mol^{-1}$ (Dinse et al., 2009), the intrinsic activation energy of the oxidation of adsorbed propylene $(Ea_{\underset{C3=}{\leftarrow}})$ could have an approximate value of around 150 $kJ \cdot mol^{-1}$ (Eq. (53)). For a more accurate estimation of $Ea_{\underset{C3=}{\leftarrow}}$, it would be necessary to determine the real value of $\Delta H_{Ads,C3=}$ for the catalyst used in this study.

Among the kinetics parameters obtained in this work for propane ODH reaction (Table 3), the most comparable values with those ones found in the literature is the activation energy of the propane activation step ($Ea_{C3} = 104 kJ/mol$), since this step is usually considered in the reaction mechanism as the RDS. However, a wide range of Ea_{C3} values for catalysts of vanadium oxide dispersed on ZrO_2 can be found in the literature, rendering meaningless any direct comparison of them (Carrero et al., 2014; Frank et al., 2007; Khodakov et al., 1998; Bottino et al., 2003; Argyle et al., 2002; Creaser and Andersson, 1996; Andersson, 1994; Grabowski, 2006; Kondratenko et al., 2005; Dinse et al., 2008; Jibril et al., 2004; Baldi et al., 1998; Routray et al., 2004; Chakraborty et al., 2015; Khodakov et al., 1999; Carrero et al., 2014; Zhang and Liu, 2019; Michaels et al., 1996; Dinse et al., 2009). Such variations among the different authors can be associated to the variability of catalysts, due to the use of different synthesis methods, supports and vanadium concentrations, which may result in different kind of vanadia surface species; as well as the wide range of different kinetic models proposed in the literature, which are sometimes oversimplified, based on inconsistent or incorrect models, and/or without physical explanation, as it could be the case of the MK expression (Vannice, 2007).

The values of $k_{\underset{C3=}{\rightarrow}}$ and $k_{Acetone}$ are much larger than k_{C3} (by 10^{10} and 10^{6} times when it is evaluated at 350 °C, respectively), resulting in negligible values of $\theta_{Isopropoxide}$ (Eq. (37)), which is consistent with the previous assumptions. Moreover, the ratio $k_{\underset{C3=}{\rightarrow}}/k_{Acetone}$ is always very high, rendering selectivity ratio values of $(k_{\underset{C3=}{\rightarrow}}/(k_{\underset{C3=}{\rightarrow}} + k_{Acetone}))$ close to 1, for the whole range of the studied temperatures (300–400 °C), with the ratio increasing even more with temperature, since $Ea_{\underset{C3=}{\rightarrow}} > Ea_{Acetone}$. This means that the fraction of converted propane that is directly oxidized to form CO_x is negligible, which is in very good accordance with results reported elsewhere (Carrero et al., 2014; Grabowski, 2006; Dinse et al., 2009). Then, most of the CO_x formed come from the oxidation of the adsorbed propylene represented by the term of $k_{App,\underset{C3=}{\leftarrow}} \cdot P_{C3=} \cdot \left(\frac{\theta_{V-OH}}{\theta_{V-O}}\right)$, where the $Ea_{App,\underset{C3=}{\leftarrow}}$ present a value of 112.0 $kJ \cdot mol^{-1}$. This latter value is higher than the activation energies of propane activation step ($Ea_{C3} = 104.1$ $kJ \cdot mol^{-1}$), and propylene formation ($Ea_{\underset{C3=}{\rightarrow}} = 91.2$ $kJ \cdot mol^{-1}$), which could mean that the selectivity to propylene would tend to be lower as temperature increases for same propane conversions, although it will also depend on the propylene partial pressure and the ratio of the surface coverages of V-O and V-OH sites.

The highest values of activation energies in Table 3 correspond to the CO and CO_2 formation steps ($Ea_{Acetate} = 180$ $kJ \cdot mol^{-1}$, $Ea_{Formate}$=140 $kJ \cdot mol^{-1}$ and $Ea_{CO2} = 116$ $kJ \cdot mol^{-1}$), which could result in a certain accumulation of acetates and formates (CO precursor species) on the catalyst surface during reaction (especially at low temperatures). Consequently, the formation of CO_2 could be induced at high temperatures as observed in a previous work (Ternero-Hidalgo et al., 2018). The high activation energies for the evolution of formate and acetate species result in low values of their respective rate constants, $k_{Formate}$ and $k_{Acetate}$, being both significantly smaller than $k_{Acetone}$ (by 10^{3} and 10^{5} times when it is evaluated at 350 °C, respectively), and resulting in appreciable

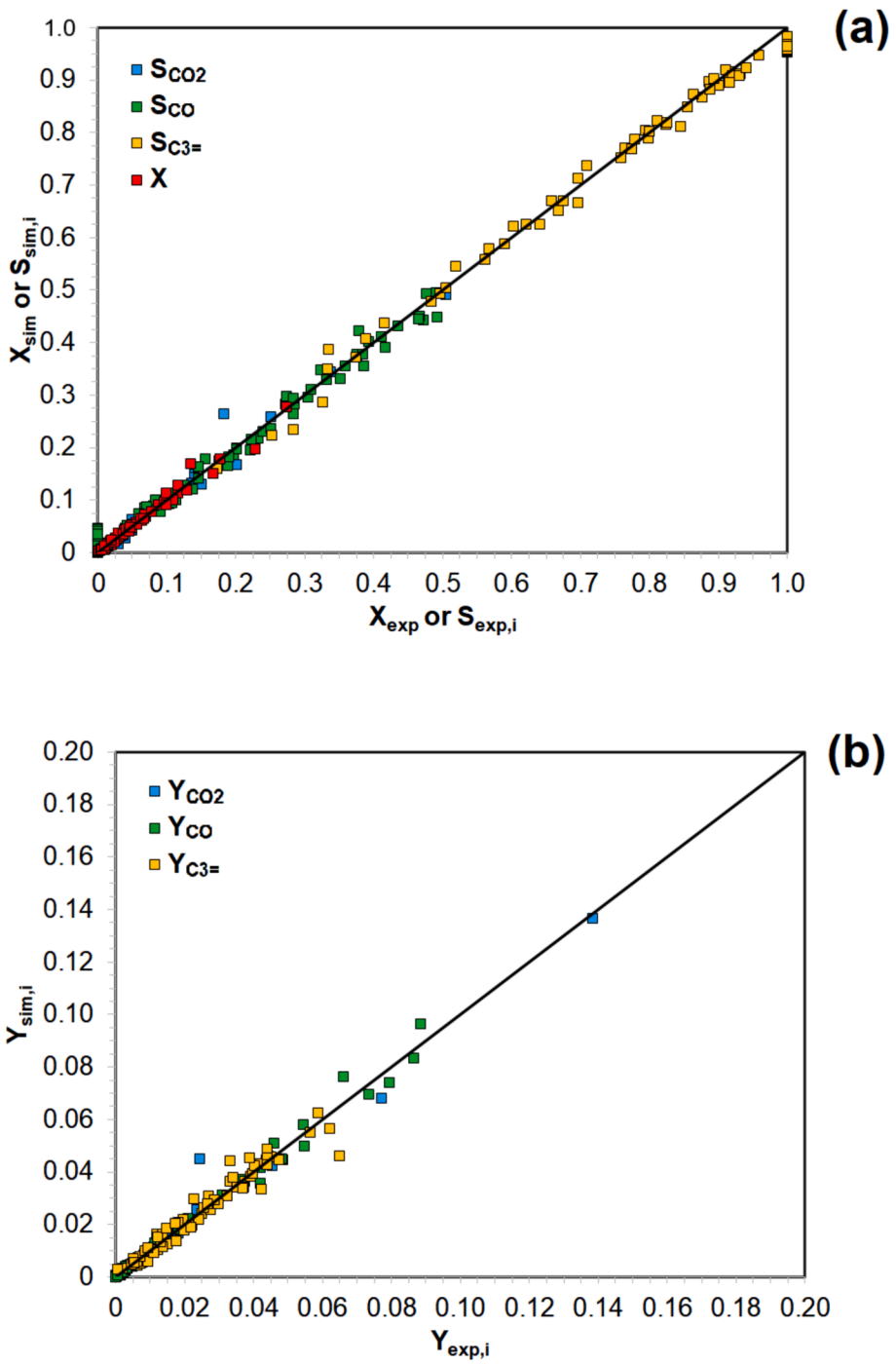

Fig. 2. Simulated propane conversion and selectivity to propylene, CO or CO_2 (X_{sim} and $S_{sim,i}$, respectively) versus their respective conversion and selectivity experimentally obtained (X_{exp} and $S_{exp,i}$, respectively).

surface coverages of formate and acetate adsorbed species, according to Eqs. (38) and (39). It can be also observed as $Ea_{Acetate}$ is larger than $Ea_{Formate}$, which is in agreement with the higher thermal stability of acetate species than formate species on the catalyst surface (Finocchio et al., 1994; Finocchio et al., 1996). In addition, it can be checked that k_{V-OH} and k_{O2} are several orders of magnitude greater than the rate constant corresponding to the RDS (k_{C3}) at 350 °C. Thus, Eqs. (41)–(43) predict that θ_{V-OH} and $\theta_{V-\square}$ are smaller than θ_{V-O} under most of the reaction conditions.

3.4. Influence of space–time

As shown in Fig. 3, the model satisfactorily describes the conversion and selectivity profiles for F-PZr-V5.0 at different space–time and temperature, since experimental and simulated data match very well for a broad range of conversion and selectivity values. As expected for propane ODH, the conversion is higher as the temperature and space–time increase (Fig. 3a), and the selectivity to propylene decreases as conversion increases (Fig. 3b). When space–time tends to very low values, propane conversion and selectivity to propylene tend to be negligible and close to 100 %, respectively. However, if the space–time tended to very high values (not shown), the conversion would be 100 % for the

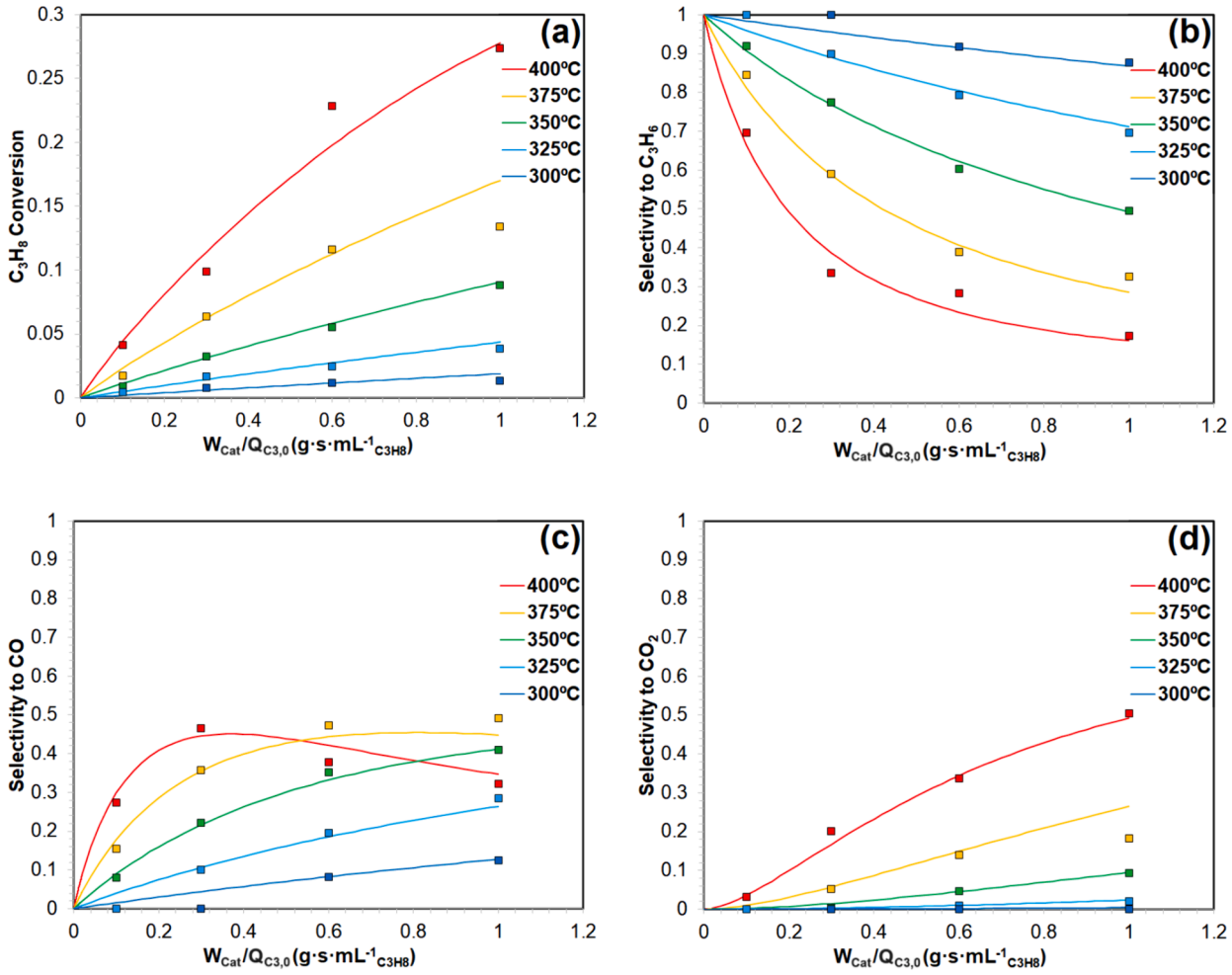

Fig. 3. Steady-state propane conversion (a), selectivity to propylene (b), CO (c) and CO_2 (d) for F-PZr-V5.0 as a function of space-times and reaction temperatures at inlet partial pressures of propane and oxygen of 0.1 atm (square dots: experimental values; solid lines: simulated values).

limiting reactant (propane or oxygen) and probably the selectivity to CO_2 could be 100 % or very high (depending on the propane/oxygen ratio). Selectivity to propylene can be close to 100 % for some conditions, such as at low propane conversions, when the fraction of $k_{\rightarrow C3=}/(k_{\rightarrow C3=}+k_{Acetone})$ has a value of ~ 1. This means that almost all the converted propane is forming, first, propylene instead of being directly oxidized to CO_x via chemisorbed acetone formation. Therefore, the gas-phase CO_x will mainly come from the consecutive combustion of the propylene, previously formed, as also reported elsewhere (Carrero et al., 2014; Grabowski, 2006; Dinse et al., 2009). Consequently, the selectivity to CO and CO_2 (Fig. 3c and 3d, respectively) is higher as the conversion increases (i.e. as the space–time and temperature increase). However, the selectivity to CO starts to decrease at high temperatures (400 °C), due to its further oxidation to CO_2.

Fig. 4 represents the estimated evolution of the surface coverages for the different adsorbed and vanadia species as a function of the space–time, temperature and propane inlet partial pressure. Concretely, Fig. 4a and 4b show the simulation of the surface coverages for a propane inlet partial pressure of 0.1 atm (same conditions than the experiments shown in Fig. 3). In general, the reduction degree of the catalyst along the fixed-bed reactor is higher as the space–time and temperature increase. This trend is evidenced by the successive loss of V-O sites and the growing appearance of surface vacancies in the VO_x lattice (V-□) (Fig. 4a), as well as the formation of more acetate and formate adsorbed species (Fig. 4b). It can also be observed that the surface coverage of V-OH sites is quite low with respect to the other vanadia species, and it decreases as space–time or temperature increases (Fig. 4b). As expected, isopropoxide species appear in negligible concentrations (Fig. 4b) (Ternero-Hidalgo et al., 2021).

It is interesting to point out that θ_{V-O} and $\theta_{V-□}$ represented most of the sites in these conditions (Fig. 4a), always covering more than the 97 % of the surface sites, being θ_{V-O} in the range of 0.60–0.90 and $\theta_{V-□}$ 0.10–0.40. Then, the catalyst studied in this work is not always fully or almost fully oxidized during reaction, in contrast to the claims made by other authors with similar catalysts, which suggest that the catalysts are fully oxidized under these operation conditions (Creaser and Andersson, 1996; Carrero et al., 2014). Note that even when the space–time tends to 0, θ_{V-O} already presents values around 0.88, which slightly decreases with temperature, indicating that these species would be the equilibrium at steady-state conditions if there was no appreciable conversion (i.e. an atmosphere of propane and oxygen without propylene and CO_x). However, as the reaction progresses (i.e. the conversion is higher), the propylene and CO formed compete with propane for the same active sites and they can be also adsorbed and further reduce the catalyst, while producing CO_x. These reactions consume much more lattice oxygen than the propylene formation, which can explain the higher reduction state of the catalyst as the space–time is higher. Therefore, the oxidation state of the catalyst will depend on the feed composition, temperature and space–time, as well as it will affect to the propane TOF, since the RDS is second-order with respect to θ_{V-O}. These results imply that the degree of catalyst reduction and consequently the TOF values could change along the fixed-bed reactor. Therefore, the calculated apparent TOF value at certain conditions will significantly depend on the overall oxidation

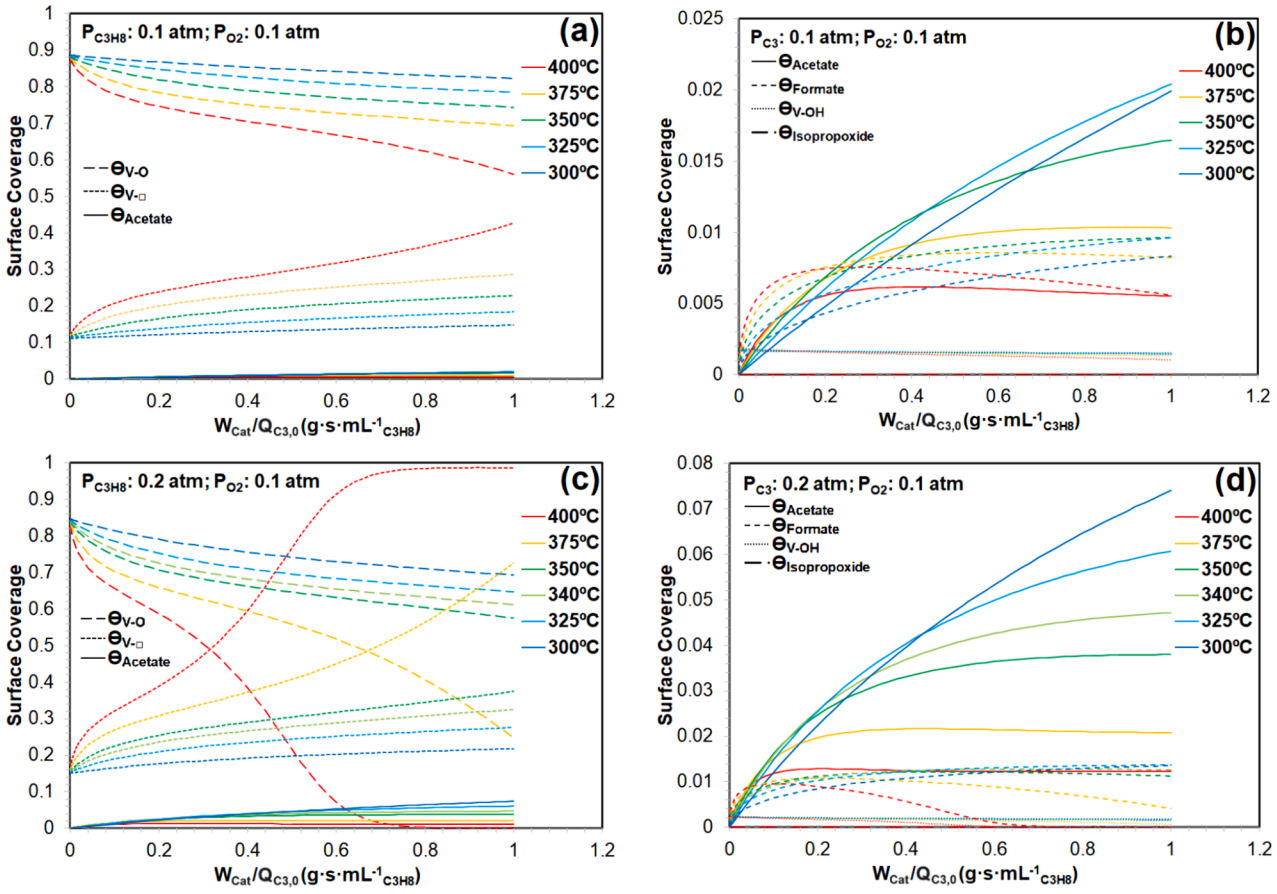

Fig. 4. Simulation of steady-state surface coverages of V-O, V-□, acetate, formate, V-OH and isopropoxide for F-PZr-V5.0 as a function of space–time and reaction temperature at inlet partial pressures of oxygen of 0.1 atm and propane of 0.1 (a,b) and 0.2 (c,d) atm.

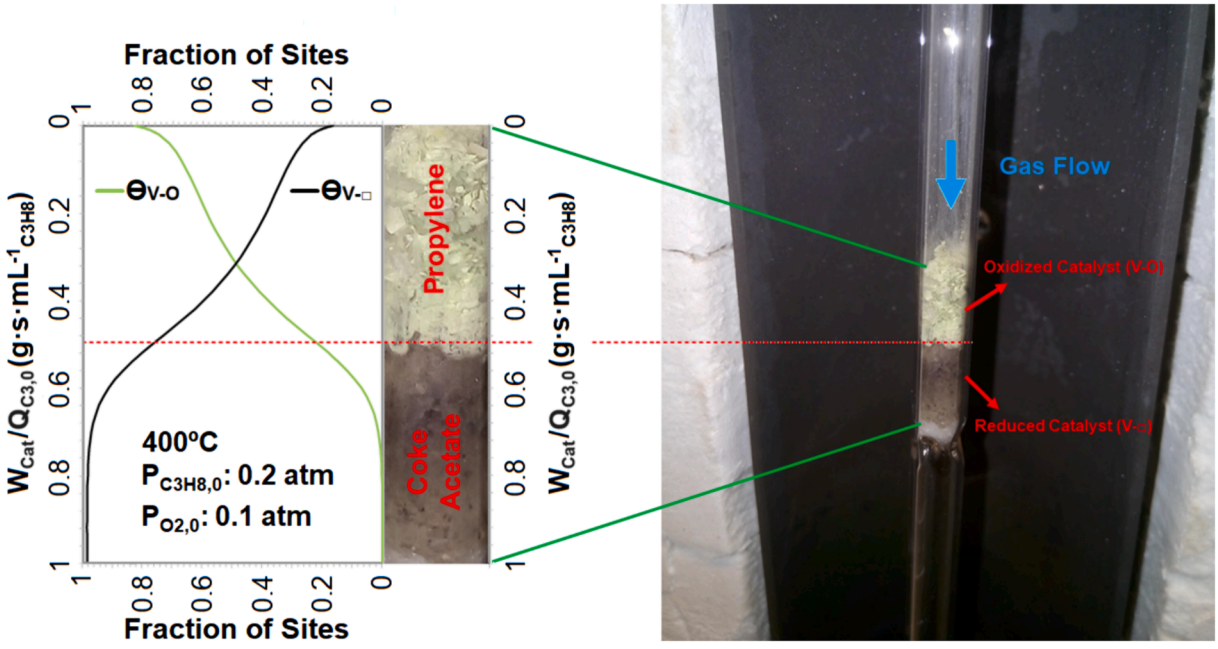

Fig. 5. (Left) simulated values of surface coverage for V-O and V-□ sites along the fixed-bed reactor and (Right) picture of the fixed-bed reactor for F-PZr-V5.0 after reaction experiment at 400 °C with a space–time of 1.0 g·s·mL$^{-1}_{C3H8}$, propane and oxygen inlet partial pressures of 0.2 and 0.1 atm, respectively.

state of the catalyst along the reactor. This appreciation was already considered by Deo et al. (Shee et al., 2006; Rao and Deo, 2007) to compare TOF values with more precision, although they used the Mars-van Krevelen expression.

TOF values have been widely used by many authors to describe the activity of catalysts in the propane ODH reaction to discern if monovanadate species are more, less or equally active than polyvanadates species. These studies have been typically based on analyzing the dependence of propane TOF values with respect to the vanadium content of the catalysts, which directly affect the proportion of polyvanadate species with respect to monovanadate ones, being higher as the vanadium surface density increases. However, different trends have been reported in the literature (Kondratenko et al., 2005; Khodakov et al., 1999; Solsona et al., 203 (2001); Christodoulakis et al., 2004; Gao et al., 2002; Shee et al., 2006; Rao and Deo, 2007; Chen et al., 2002; Viparelli et al., 1999), which have been studied in an extensive review reported by Carrero et al. (Carrero et al., 2014), reaching to the conclusion that surface VO_4 monomer possesses the same TOF as the surface VO_4 polymer. According to the results predicted by the kinetic model proposed in this work, this apparent non-universal behavior could be related to the different vanadium content in the catalysts. In this context, for a catalyst with higher vanadium content (i.e. more active sites), the propane conversions will be higher for same reaction conditions, resulting in a deeper degree of reduction of the catalyst as above explained. Consequently, the observed TOF could be lower in the catalyst with higher vanadium content, even though the intrinsic catalytic activity of the latter one is higher or at least comparable to that of the catalyst with lower vanadium content. Therefore, the comparison of propane TOF data of two catalysts should be carried out under the same experimental conditions. Otherwise, the conditions for the catalytic measurements should be clearly stated, or it is possible to lead to wrong conclusions. Furthermore, unless the catalysts are always fully oxidized under reaction conditions, the use of only propane TOF values are not enough to get solid conclusions about the activity of these kind of catalysts, due to the non-linear variation of the catalyst oxidation state, which presents a complex dependence on many factors because of the reaction mechanism nature.

Fig. 4c and 4d represent the steady-state surface coverages, but for a higher propane inlet partial pressure, 0.2 atm. In this case, a similar catalytic behavior is observed, with the above-mentioned features being found in a greater extent. In fact, Fig. 4c shows that the catalyst surface can be totally reduced at temperatures above 375 °C for large space times, which always matches with total consumption of the oxygen in the gas phase (not shown in the figure). For instance, it should be noted that the molecular oxygen in the gas phase is totally consumed around the space–time of 0.7 $g{\cdot}s{\cdot}mL^{-1}_{C3H8}$ at 400 °C, which explains the subsequent total reduction of the catalyst from this position, therefore, leaving without activity more than half of the catalyst. At larger space-times, all the concentrations on the surface and in the gas phase remain constant, denoting the depletion of that part of the catalyst. It can be observed that $\theta_{V-\square}$ is ~ 0.99, $\theta_{Acetate}$ is ~ 0.01 and the surface coverage of the remaining species are negligible. It is important to highlight that the remaining acetate species can stay on the surface because they would require lattice oxygen to evolve as CO, while formate surface species are completely removed due to that they are able to evolve without the presence of lattice oxygen (Scheme 1).

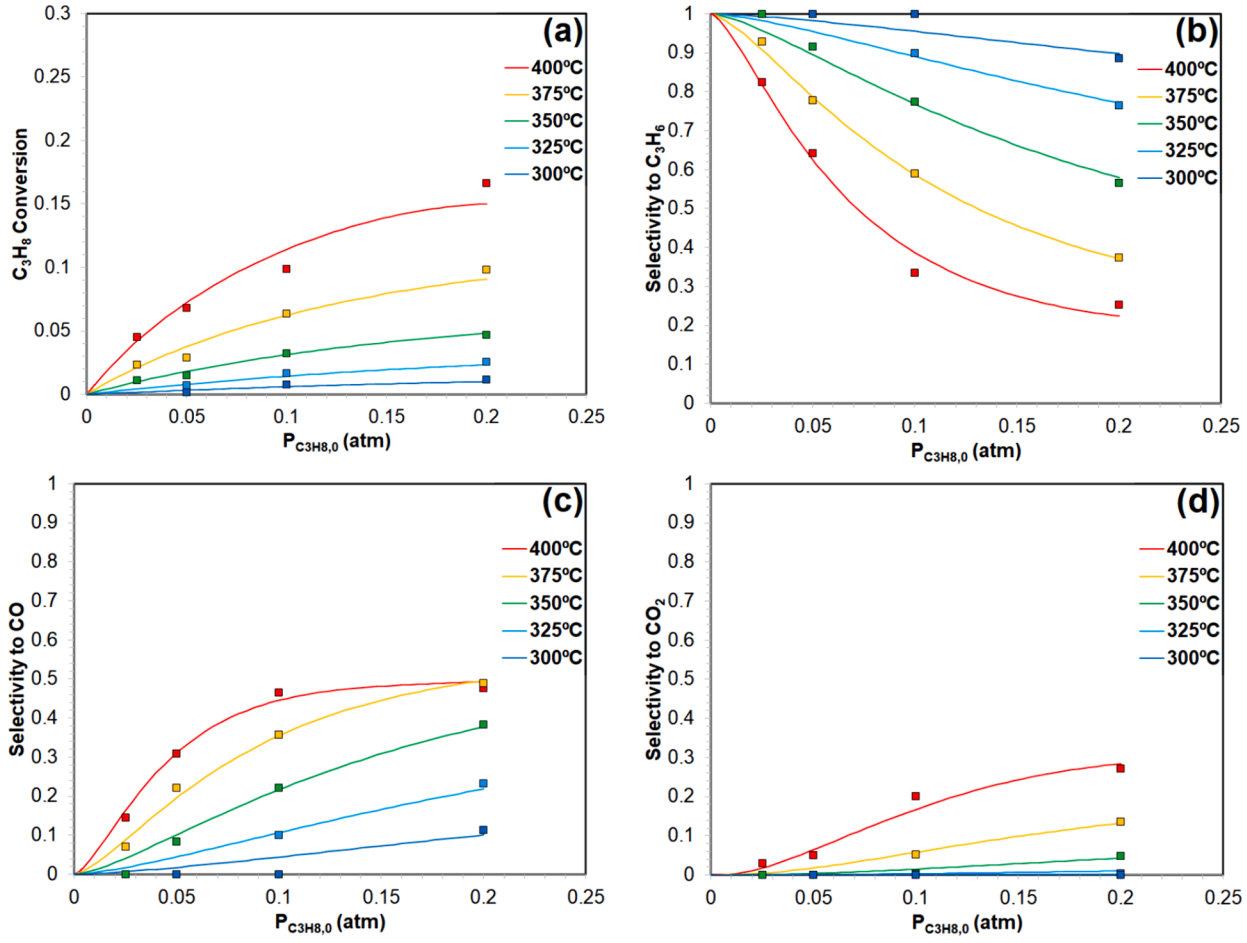

Fig. 6. Steady-state propane conversion (a), selectivity to propylene (b), CO (c) and CO_2 (d) for F-PZr-V5.0 versus propane inlet partial pressure and reaction temperature at space–time of 0.3 $g{\cdot}s{\cdot}mL^{-1}_{C3H8}$ and oxygen inlet partial pressure of 0.1 (square symbols: experimental values; solid lines: simulated values).

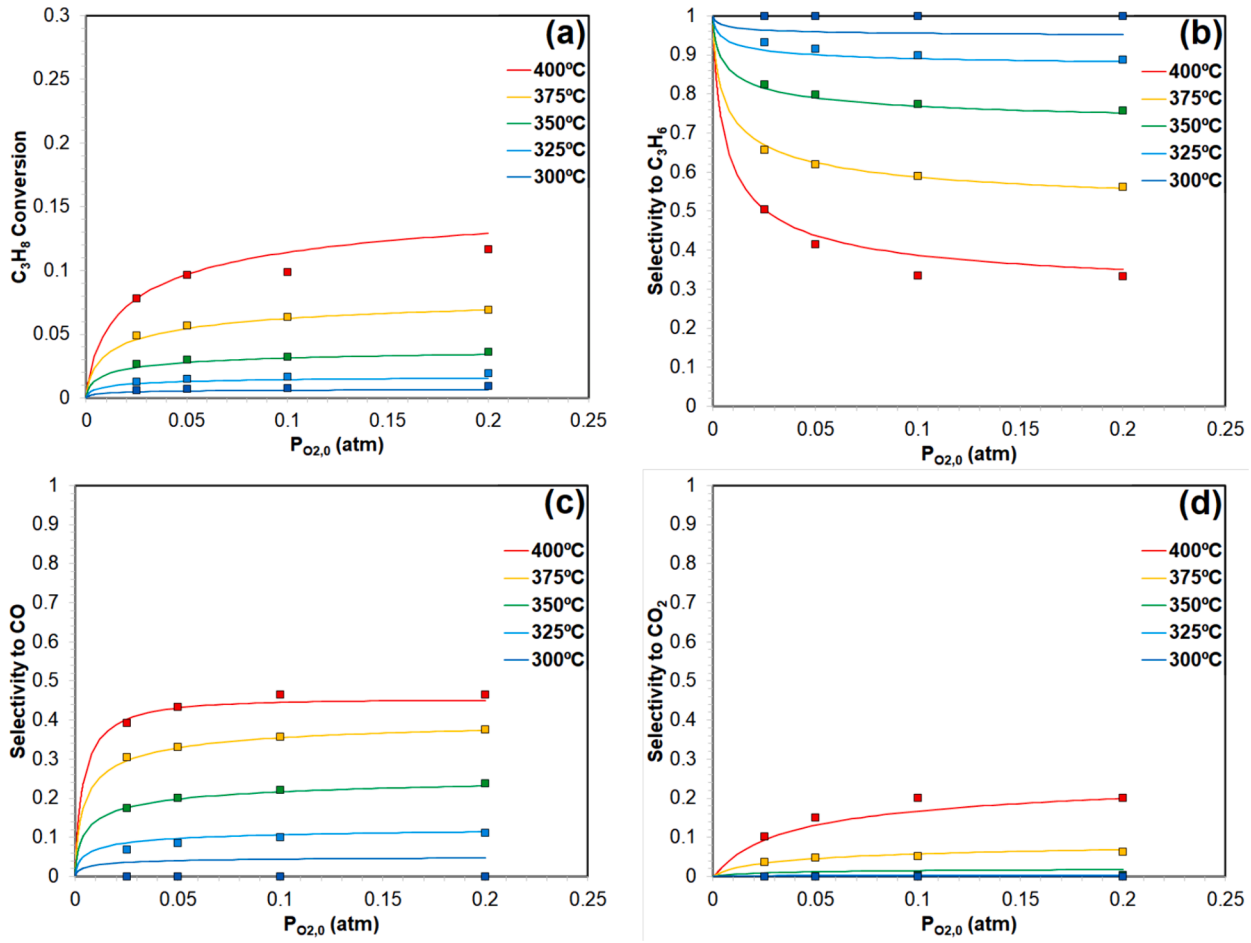

Fig. 7. Steady-state propane conversion (a), selectivity to propylene (b), CO (c) and CO_2 (d) for F-PZr-V5.0 versus oxygen inlet partial pressure and reaction temperature at space–time of 0.3 g·s·mL$^{-1}_{C3H8}$ and propane inlet partial pressure of 0.1 atm (square symbols: experimental values; solid lines: simulated values).

To support this hypothesis, Fig. 5 shows a picture that was taken after performing the experiment at 400 °C under the same conditions used for the experiments depicted in Fig. 4c and 4d. Interestingly, the catalyst become dark in color when is reduced, maybe due to coke deposition that occurs when the catalyst is in a high reduction degree. In fact, the FTIR and Raman spectra, reported in a previous work, mainly showed the presence of acetates and coke, respectively, as the remaining adsorbed species when the catalyst was totally reduced (Ternero-Hidalgo et al., 2021). Fig. 5 also collects the simulated values of surface coverage for V-O and V-□ sites along the fixed-bed reactor. A striking match is observed between the change of color in the catalytic bed and the space–time where V-O sites start to be almost exhausted ($\theta_{V-O} \approx 0.2$), according to the simulation. The picture also reveals a flat radial velocity profile of the gas flow along the catalyst, verifying the plug-flow behavior of the reactor. Therefore, this result confirms the presumptions made in the kinetic mechanism, as well as it evidences the high accuracy of the proposed kinetic model.

3.5. *Influence of inlet partial pressure of propane and oxygen*

Figs. 6 and 7 show conversion-selectivity profiles, while Fig. 8 represents simulated surface coverages of vanadia and adsorbed species, as a function of temperature and inlet partial pressures of propane or oxygen for F-PZr-V5.0. A good agreement is observed between the experimental and simulated values of conversion and selectivity obtained in the whole range studied of propane and oxygen inlet partial pressures (Figs. 6 and 7, respectively). As expected, the conversion and selectivity values markedly present a stronger influence with the inlet partial pressure of propane than with oxygen. Accordingly, the evolutions of the surface coverages of the vanadia and adsorbed species in function of propane or oxygen inlet partial pressure are also very different (Fig. 8).

The variations in space–time and propane inlet partial pressure provide a similar outcome on the conversion-selectivity profiles as can be deduced from the comparison of Figs. 3 and 6. The conversion increases as the propane inlet partial pressure increases, and consequently the selectivity decreases. However, there are some differences regarding the surface species, as can be observed when Fig. 4a and 4b are compared to Fig. 8a and 8b, respectively. First, the increase of propane inlet partial pressure tends to promote the reduction of the catalyst in more extent than the increase of space–time, denoted by the faster decrease of lattice oxygen concentration and the faster increase of adsorbed species, mainly as acetate. Second, as expected, when the propane inlet pressure tends to 0, θ_{V-O} always becomes 1, due to the catalyst would be under an oxidant atmosphere without propane (see Fig. 8a).

Moreover, it can be observed in Figs. 7, 8c and 8d that there exists a strong influence of the oxygen at low partial pressures on the conversion-selectivity profiles and on the surface coverages of vanadia and adsorbed species, respectively. This influence becomes less important from a certain value of oxygen concentration in the gas phase. In these conditions, the kinetic of the reaction becomes pseudo-zero order with respect to oxygen. However, the presence of oxygen in the gas phase is still necessary for the reoxidation of the catalyst to keep the catalytic cycle, otherwise the activity would be null as predicted in Fig. 7a, since the active sites would be exhausted (i.e. $\theta_{V-O} \approx 0$), as shown in Fig. 8c.

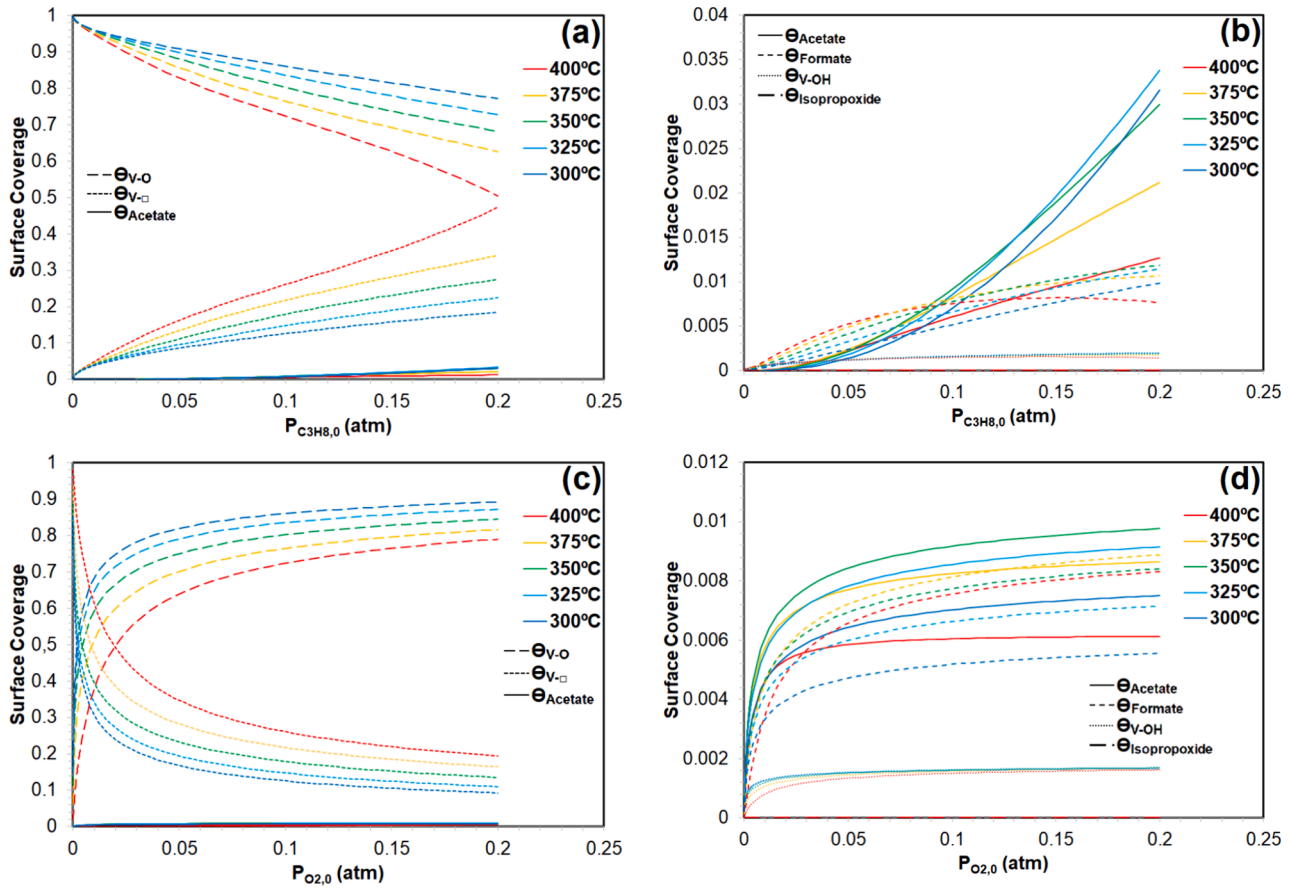

Fig. 8. Simulation of steady-state surface coverages of V-O, V-□, acetate, formate, V-OH and isopropoxide for F-PZr-V5.0 versus reaction temperature and inlet partial pressures of propane (a,b) or oxygen (c,d) at space–time of 0.3 g·s·mL$^{-1}_{C3H8}$.The inlet partial pressure of oxygen or propane was 0.1 atm in (a,b) and (c,d), respectively.

The fact that the RDS is second-order with respect to θ_{V-O} (Eq. (5)) means that the propane conversion profile will be determined in part by the surface coverage of the lattice oxygen, which is strongly linked to the reaction conditions according to Eq. (43). For instance, the evolution of θ_{V-O} as a function of oxygen inlet partial pressure predicted in Fig. 8c can explain why the propane conversion sharply change at low oxygen concentrations, while it is almost constant at higher oxygen inlet partial pressures (Fig. 7). Moreover, it should be noted that the model predicts that the catalyst is not fully oxidized even for the highest oxygen inlet partial pressures used in this work (Fig. 8c). This means that, although the reaction is pseudo-zero order with respect to the oxygen partial pressure under certain conditions, the catalyst may not be nearly saturated with oxygen. Many authors have reported zero-order dependence of oxygen in the ODH reaction (Khodakov et al., 1998; Argyle et al., 2002; Creaser and Andersson, 1996; Khodakov et al., 1999; Carrero et al., 2014; Zhang and Liu, 2019; Michaels et al., 1996; Dinse et al., 2009), assuming that the reoxidation reaction of the catalyst is several orders faster than the reduction reaction, and then, sometimes it has also been considered that the catalyst is fully oxidized under reaction conditions (Creaser and Andersson, 1996; Carrero et al., 2014), an assertion that needs to be carefully examined under these operation conditions. The model herein proposed contradicts these assumptions, since it will depend on each catalyst nature and reaction conditions.

4. Conclusions

This work proposed a kinetic model for the ODH reaction, which satisfactorily predicts the conversion and selectivity profiles, and the surface coverage of the different species present on a vanadium oxide-based submicron fiber catalyst, for all the studied conditions of temperature, space–time and inlet partial pressures of propane and oxygen, covering a broad range of conversion and selectivity values. The first hydrogen abstraction from propane is the rate determining step (RDS) and the calculated activation energy is 104 kJ·mol^{-1}, which is quite different from some values reported in the literature, probably related to the use of mathematical fitting functions without physical relevance, like Mars-van Krevelen expression or oversimplified models.

The conversion and selectivity values, as well as the surface coverages or fraction of sites of the different species, present a strong dependence on temperature, space–time and propane inlet partial pressure. However, the influence of oxygen concentration is only important at low oxygen partial pressures, becoming pseudo-zero order dependence (i.e. independent) with respect to oxygen concentration once exceeded a certain value. Moreover, the model predicts that the catalyst used in this work is not fully oxidized under different reaction conditions, even for the highest oxygen inlet partial pressures used, and neither when the space–time tends to zero (i.e. negligible conversions). This surprising claim has been experimentally verified, showing a remarkable agreement between the oxidation/reduction state of the catalytic bed experimentally observed and the one predicted by the model. These results suggest that although the reaction is pseudo-zero order with respect to oxygen for a broad range of conditions, the catalyst may not be fully oxidized, even though the reoxidation reaction of the catalyst may be much faster than the reduction. Then, the simplification about the catalyst is always fully oxidized to simplify the equations could be wrongly assumed. In fact, the model predicts that the catalyst oxidation state under reaction conditions will depend on its intrinsic chemical nature, the feed composition, temperature and

space–time. Furthermore, the comparison among catalysts in terms of propane TOF values is not straightforward, unless the catalysts are fully oxidized under reaction conditions.

CRediT authorship contribution statement

Juan José Ternero-Hidalgo: Writing – original draft, Investigation, Formal analysis. **Ramiro Ruiz-Rosas:** Validation, Supervision, Software. **Juana María Rosas:** Project administration, Writing – review & editing, Supervision. **María Olga Guerrero-Pérez:** Supervision, Project administration. **José Rodríguez-Mirasol:** Writing – review & editing, Supervision, Project administration, Funding acquisition. **Tomás Cordero:** Writing – review & editing, Visualization, Supervision, Conceptualization.

Declaration of competing interest

The authors declare that they have no known competing financial interests or personal relationships that could have appeared to influence the work reported in this paper.

Data availability

Data will be made available on request.

Acknowledgements

This work was supported by MCIN (PID2022-140844OB-I00 and TED2021-131324B-C21) and European Union "NextGenerationEU"/PRTR (MCIN/AEI/10.13039/501100011033). Funding for open access charge: Universidad de Malaga / CBUA. J.J.T.H. acknowledges the assistance of the Ministry of Economy and Competitiveness of Spain for the award of a FPI Grant [BES-2013-064425].

Appendix A. Supplementary data

Supplementary data to this article can be found online at https://doi.org/10.1016/j.ces.2024.120192.

References

Agarwal, A., Sengupta, D., El-Halwagi, M., 2018. Sustainable Process Design Approach for On-Purpose Propylene Production and Intensification. ACS Sustain. Chem. Eng. 6, 2407–2421. https://doi.org/10.1021/acssuschemeng.7b03854.

Amghizar, I., Vandewalle, L.A., Van Geem, K.M., Marin, G.B., 2017. New Trends in Olefin Production. Engineering. 3, 171–178. https://doi.org/10.1016/J.ENG.2017.02.006.

Andersson, S.L.T., 1994. Kinetic study of the oxidative dehydrogenation of propane over vanadia supported on amorphous AlPO4. Appl. Catal. Gen. 112, 209–218. https://doi.org/10.1016/0926-860X(94)80220-3.

Argyle, M.D., Chen, K., Bell, A.T., Iglesia, E., 2002. Effect of Catalyst Structure on Oxidative Dehydrogenation of Ethane and Propane on Alumina-Supported Vanadia. J. Catal. 208, 139–149. https://doi.org/10.1006/jcat.2002.3570.

Baldi, M., Finocchio, E., Pistarino, C., Busca, G., 1998. Evaluation of the mechanism of the oxy-dehydrogenation of propane over manganese oxide. Appl. Catal. Gen. 173, 61–74. https://doi.org/10.1016/S0926-860X(98)00129-X.

Balogun, M.L., Adamu, S., Ba-Shammakh, M.S., Hossain, M.M., 2021. Promotional effects of CO2 on the oxidative dehydrogenation of propane over mesoporous VOX/γAl2O3 catalysts. J. Ind. Eng. Chem. 96, 82–97. https://doi.org/10.1016/j.jiec.2020.12.022.

Berger, R.J., Pérez-Ramírez, J., Kapteijn, F., Moulijn, J.A., 2002. Catalyst performance testing: The influence of catalyst bed dilution on the conversion observed. Chem. Eng. J. 90, 173–183. https://doi.org/10.1016/S1385-8947(02)00078-5.

Bottino, A., Capannelli, G., Comite, A., Storace, S., Di Felice, R., 2003. Kinetic investigations on the oxidehydrogenation of propane over vanadium supported on γ-Al2O3. Chem. Eng. J. 94, 11–18. https://doi.org/10.1016/S1385-8947(03)00003-2.

Brazdil, J.F., 2006. Strategies for the selective catalytic oxidation of alkanes. Top. Catal. 38, 289–294. https://doi.org/10.1007/s11244-006-0027-4.

Busca, G., Finocchio, E., Lorenzelli, V., Ramis, G., Baldi, M., 1999. IR studies on the activation of C-H hydrocarbon bonds on oxidation catalysts. Catal. Today. 49, 453–465. https://doi.org/10.1016/S0920-5861(98)00441-6.

Carrero, C., Kauer, M., Dinse, A., Wolfram, T., Hamilton, N., Trunschke, A., Schlögl, R., Schomäcker, R., 2014. High performance (VOx)n–(TiOx)m/SBA-15 catalysts for the oxidative dehydrogenation of propane, Catal. Sci. Technol. 4, 786–794. https://doi.org/10.1039/C3CY00625E.

Carrero, C.A., Schloegl, R., Wachs, I.E., Schomaecker, R., 2014. Critical Literature Review of the Kinetics for the Oxidative Dehydrogenation of Propane over Well-Defined Supported Vanadium Oxide Catalysts. ACS Catal. 4, 3357–3380. https://doi.org/10.1021/cs5003417.

Cavani, F., Ballarini, N., Cericola, A., 2007. Oxidative dehydrogenation of ethane and propane: How far from commercial implementation? Catal. Today. 127, 113–131. https://doi.org/10.1016/j.cattod.2007.05.009.

Chakraborty, S., Nayak, S.C., Deo, G., 2015. TiO2/SiO2 supported vanadia catalysts for the ODH of propane. Catal. Today. 254, 62–71. https://doi.org/10.1016/j.cattod.2015.01.047.

Chen, K., Khodakov, A., Yang, J., Bell, A.T., Iglesia, E., 1999. Isotopic Tracer and Kinetic Studies of Oxidative Dehydrogenation Pathways on Vanadium Oxide Catalysts. J. Catal. 186, 325–333. https://doi.org/10.1006/jcat.1999.2510.

Chen, K., Bell, A.T., Iglesia, E., 2000. Kinetics and Mechanism of Oxidative Dehydrogenation of Propane on Vanadium, Molybdenum, and Tungsten Oxides. J. Phys. Chem. b. 104, 1292–1299. https://doi.org/10.1021/jp9933875.

Chen, K., Bell, A.T., Iglesia, E., 2002. The Relationship between the Electronic and Redox Properties of Dispersed Metal Oxides and Their Turnover Rates in Oxidative Dehydrogenation Reactions. J. Catal. 209, 35–42. https://doi.org/10.1006/jcat.2002.3620.

Christodoulakis, A., Machli, M., Lemonidou, A.A., Boghosian, S., 2004. Molecular structure and reactivity of vanadia-based catalysts for propane oxidative dehydrogenation studied by in situ Raman spectroscopy and catalytic activity measurements. J. Catal. 222, 293–306. https://doi.org/10.1016/j.jcat.2003.10.007.

A. Corma, J.M. López-Nieto, N. Paredes, M. Pérez, Y. Shen, H. Cao, S.L. Suib, Oxidative Dehydrogenation Of Propane Over Supported-Vanadium Oxide Catalysts, in: P. Ruiz, B. Delmon (Eds.), Stud. Surf. Sci. Catal., Elsevier, 1992: pp. 213–220. https://doi.org/10.1016/S0167-2991(08)61673-0.

Creaser, D., Andersson, B., 1996. Oxidative dehydrogenation of propane over V-Mg-O: kinetic investigation by nonlinear regression analysis. Appl. Catal. Gen. 141, 131–152. https://doi.org/10.1016/0926-860X(96)00029-4.

Dinse, A., Frank, B., Hess, C., Habel, D., Schomäcker, R., 2008. Oxidative dehydrogenation of propane over low-loaded vanadia catalysts: Impact of the support material on kinetics and selectivity. J. Mol. Catal. Chem. 289, 28–37. https://doi.org/10.1016/j.molcata.2008.04.007.

Dinse, A., Khennache, S., Frank, B., Hess, C., Herbert, R., Wrabetz, S., Schlögl, R., Schomäcker, R., 2009. Oxidative dehydrogenation of propane on silica (SBA-15) supported vanadia catalysts: A kinetic investigation. J. Mol. Catal. Chem. 307, 43–50. https://doi.org/10.1016/j.molcata.2009.03.008.

Dong, S., Altvater, N.R., Mark, L.O., Hermans, I., 2021. Assessment and comparison of ordered & non-ordered supported metal oxide catalysts for upgrading propane to propylene. Appl. Catal. Gen. 617, 118121 https://doi.org/10.1016/j.apcata.2021.118121.

Finocchio, E., Busca, G., Lorenzelli, V., Willey, R.J., 1994. FTIR studies on the selective oxidation and combustion of light hydrocarbns at metal oxide surfaces. Propane and propene oxidation on MgCr2O4, J. Chem. Soc. Faraday Trans. 90, 3347–3356. https://doi.org/10.1039/FT9949003347.

Finocchio, E., Busca, G., Lorenzelli, V., Escribano, V.S., 1996. FTIR studies on the selective oxidation and combustion of light hydrocarbons at metal oxide surfaces. part 2. —propane and propene oxidation on Co3O4. J. Chem. Soc Faraday Trans. 92, 1587–1593. https://doi.org/10.1039/FT9969201587.

Frank, B., Dinse, A., Ovsitser, O., Kondratenko, E.V., Schomäcker, R., 2007. Mass and heat transfer effects on the oxidative dehydrogenation of propane (ODP) over a low loaded VOx/Al2O3 catalyst. Appl. Catal. Gen. 323, 66–76. https://doi.org/10.1016/j.apcata.2007.02.006.

Gao, X., Jehng, J.-M., Wachs, I.E., 2002. In Situ UV–vis–NIR Diffuse Reflectance and Raman Spectroscopic Studies of Propane Oxidation over ZrO2-Supported Vanadium Oxide Catalysts. J. Catal. 209, 43–50. https://doi.org/10.1006/jcat.2002.3635.

Grabowski, R., 2006. Kinetics of Oxidative Dehydrogenation of C2–C3 Alkanes on Oxide Catalysts. Catal. Rev. 48, 199–268. https://doi.org/10.1080/01614940600631413.

Grasselli, R.K., 1999. Advances and future trends in selective oxidation and ammoxidation catalysis. Catal. Today. 49, 141–153. https://doi.org/10.1016/S0920-5861(98)00418-0.

Guerrero-Pérez, M.O., 2017. Supported, bulk and bulk-supported vanadium oxide catalysts: A short review with an historical perspective. Catal. Today. 285, 226–233. https://doi.org/10.1016/j.cattod.2017.01.037.

Jibril, B.Y., Al-Zahrani, S.M., Abasaeed, A.E., Hughes, R., 2004. Propane oxidative dehydrogenation on Cs-doped Cr-Mo-Al-O catalyst: kinetics and mechanism. Chem. Eng. J. 103, 59–67. https://doi.org/10.1016/j.cej.2004.03.006.

Khodakov, A., Yang, J., Su, S., Iglesia, E., Bell, A.T., 1998. Structure and properties of vanadium oxide-zirconia catalysts for propane oxidative dehydrogenation. J. Catal. 177, 343–351. https://doi.org/10.1006/jcat.1998.2143.

Khodakov, A., Olthof, B., Bell, A.T., Iglesia, E., 1999. Structure and Catalytic Properties of Supported Vanadium Oxides: Support Effects on Oxidative Dehydrogenation Reactions. J. Catal. 181, 205–216. https://doi.org/10.1006/jcat.1998.2295.

Kondratenko, E.V., Baerns, M., 2001. Catalytic oxidative dehydrogenation of propane in the presence of O2 and N2O—the role of vanadia distribution and oxidant activation. Appl. Catal. Gen. 222, 133–143. https://doi.org/10.1016/S0926-860X(01)00836-5.

Kondratenko, E.V., Cherian, M., Baerns, M., Su, D., Schlögl, R., Wang, X., Wachs, I.E., 2005. Oxidative dehydrogenation of propane over V/MCM-41 catalysts: comparison of O2 and N2O as oxidants. J. Catal. 234, 131–142. https://doi.org/10.1016/j.jcat.2005.05.025.

J. Lazonby, Propene (Propylene), (n.d.). http://www.essentialchemicalindustry.org/chemicals/propene.html (accessed December 20, 2023).
Liu, Y.-M., Cao, Y., Zhu, K.-K., Yan, S.-R., Dai, W.-L., He, H.-Y., Fan, K.-N., 2002. Highly efficient VOx/SBA-15 mesoporous catalysts for oxidative dehydrogenation of propane. Chem. Commun. 2832–2833. https://doi.org/10.1039/B208177F.
Liu, Y.-M., Cao, Y., Yi, N., Feng, W.-L., Dai, W.-L., Yan, S.-R., He, H.-Y., Fan, K.-N., 2004. Vanadium oxide supported on mesoporous SBA-15 as highly selective catalysts in the oxidative dehydrogenation of propane. J. Catal. 224, 417–428. https://doi.org/10.1016/j.jcat.2004.03.010.
Mars, P., van Krevelen, D.W., 1954. Oxidations carried out by means of vanadium oxide catalysts. Chem. Eng. Sci. 3, 41–59. https://doi.org/10.1016/S0009-2509(54)80005-4.
Michaels, J.N., Stern, D.L., Grasselli, R.K., 1996. Oxydehydrogenation of propane over Mg-V-Sb-oxide catalysts. II. Reaction kinetics and mechanism. Catal. Lett. 42, 139–148. https://doi.org/10.1007/BF00810679.
Pérez-Ramírez, J., Berger, R.J., Mul, G., Kapteijn, F., Moulijn, J.A., 2000. Six-flow reactor technology a review on fast catalyst screening and kinetic studies. Catal. Today. 60, 93–109. https://doi.org/10.1016/S0920-5861(00)00321-7.
Rao, T.V.M., Deo, G., 2007. Kinetic parameter analysis for propane ODH: V2O5/Al2O3 and MoO3/Al2O3 catalysts. AIChE J. 53, 1538–1549. https://doi.org/10.1002/aic.11176.
Reichelt, E., Heddrich, M.P., Jahn, M., Michaelis, A., 2014. Fiber based structured materials for catalytic applications. Appl. Catal. Gen. 476, 78–90. https://doi.org/10.1016/j.apcata.2014.02.021.
Rogg, S., Hess, C., 2021. CO2 as a soft oxidant for propane oxidative dehydrogenation: A mechanistic study using operando UV Raman spectroscopy. J. CO2 Util. 50, 101604 https://doi.org/10.1016/j.jcou.2021.101604.
Routray, K., Reddy, K.R.S.K., Deo, G., 2004. Oxidative dehydrogenation of propane on V2O5/Al2O3 and V2O5/TiO2 catalysts: understanding the effect of support by parameter estimation. Appl. Catal. Gen. 265, 103–113. https://doi.org/10.1016/j.apcata.2004.01.006.
Schumacher, L., Pfeiffer, J., Shen, J., Gutmann, T., Breitzke, H., Buntkowsky, G., Hofmann, K., Hess, C., 2023. Collaborative Mechanistic Effects between Vanadia and Titania during the Oxidative Dehydrogenation of Propane Investigated by Operando and Transient Spectroscopies. ACS Catal. 13, 8139–8160. https://doi.org/10.1021/acscatal.3c01404.
Schumacher, L., Shen, J., Hofmann, K., Hess, C., 2023. (2024), Rational design of vanadia-based propane ODH catalysts: A multiple operando spectroscopic investigation of VOx/TiO2/CeO2. Catal. Today. 426, 114387 https://doi.org/10.1016/j.cattod.2023.114387.
Shee, D., Rao, T.V.M., Deo, G., 2006. Kinetic parameter estimation for supported vanadium oxide catalysts for propane ODH reaction: Effect of loading and support. Catal. Today. 118, 288–297. https://doi.org/10.1016/j.cattod.2006.07.017.
Singh, R., Nayak, S.C., Singh, R., Deo, G., 2024. O2 and CO2 assisted oxidative dehydrogenation of propane using ZrO2 supported vanadium and chromium oxide catalysts. Catal. Today. 432, 114617 https://doi.org/10.1016/j.cattod.2024.114617.
Solsona, B., Blasco, T., López Nieto, J.M., Peña, M.L., Rey, F., Vidal-Moya, A., 2001. Vanadium oxide supported on mesoporous MCM-41 as selective catalysts in the oxidative dehydrogenation of alkanes. J. Catal. 203, 443–452. https://doi.org/10.1006/jcat.2001.3326.
Ternero-Hidalgo, J.J., Torres-Liñán, J., Guerrero-Pérez, M.O., Rodríguez-Mirasol, J., Cordero, T., 2018. Electrospun vanadium oxide based submicron diameter fiber catalysts. Part I: Preparation procedure and propane ODH application. Catal. Today. 325, 131–143. https://doi.org/10.1016/j.cattod.2018.10.073.
Ternero-Hidalgo, J.J., Guerrero-Pérez, M.O., Rodríguez-Mirasol, J., Cordero, T., 2018. Electrospun vanadium oxide based submicron diameter fiber catalysts. part II: Effect of chemical formulation and dopants. Catal. Today. 325, 144–150. https://doi.org/10.1016/j.cattod.2018.10.072.
Ternero-Hidalgo, J.J., Guerrero-Pérez, M.O., Rodríguez-Mirasol, J., Cordero, T., Bañares, M.A., Portela, R., Bazin, P., Clet, G., Daturi, M., 2020. Operando reactor-cell with simultaneous transmission FTIR and raman characterization (IRRaman) for the study of gas-phase reactions with solid catalysts. Anal. Chem. 92, 5100–5106. https://doi.org/10.1021/acs.analchem.9b05473.
Ternero-Hidalgo, J.J., Daturi, M., Clet, G., Bazin, P., Bañares, M.A., Portela, R., Guerrero-Pérez, M.O., Rodríguez-Mirasol, J., Cordero, T., 2021. A simultaneous operando FTIR & Raman study of propane ODH mechanism over V-Zr-O catalysts. Catal. Today. https://doi.org/10.1016/j.cattod.2021.06.012.
The Propylene Gap: How Can It Be Filled? - American Chemical Society, (2018). https://web.archive.org/web/20180507154000/https:/www.acs.org/content/acs/en/pressroom/cutting-edge-chemistry/the-propylene-gap-how-can-it-be-filled.html (accessed December 21, 2021).
Vannice, M.A., 2005. Kinetics of catalytic reactions. Springer, New York.
Vannice, M.A., 2007. An analysis of the Mars–van Krevelen rate expression. Catal. Today. 123, 18–22. https://doi.org/10.1016/j.cattod.2007.02.002.
Viparelli, P., Ciambelli, P., Lisi, L., Ruoppolo, G., Russo, G., Volta, J.C., 1999. Oxidative dehydrogenation of propane over vanadium and niobium oxides supported catalysts. Appl. Catal. Gen. 184, 291–301. https://doi.org/10.1016/S0926-860X(99)00104-0.
Zhang, S., Liu, H., 2019. Oxidative dehydrogenation of propane over Mg-V-O oxides supported on MgO-coated silica: Structural evolution and catalytic consequence. Appl. Catal. Gen. 573, 41–48. https://doi.org/10.1016/j.apcata.2019.01.012.